

Comparison of Anomaly Detectors: Context Matters

Vít Škvára, Jan Franců, Matěj Zorek, Tomáš Pevný, *Member, IEEE*, Václav Šmídl, *Member, IEEE*

Abstract—Deep generative models are challenging the classical methods in the field of anomaly detection nowadays. Every new method provides evidence of outperforming its predecessors, often with contradictory results. The objective of this comparison is twofold: comparison of anomaly detection methods of various paradigms, and identification of sources of variability that can yield different results. The methods were compared on popular tabular and image datasets. While the one class support-vector machine (OC-SVM) had no rival on the tabular datasets, the best results on the image data were obtained either by a feature-matching GAN or a combination of variational autoencoder (VAE) and OC-SVM, depending on the experimental conditions. The main sources of variability that can influence the performance of the methods were identified to be: the range of searched hyper-parameters, the methodology of model selection, and the choice of the anomalous samples. All our code and results are available for download.

I. INTRODUCTION

DEEP generative models are gaining popularity in anomaly detection since the introduction of the Variational Autoencoder (VAE) [43]. The number of modifications and extensions of VAE or generative adversarial networks (GAN) [31] is sharply increasing, each claiming superiority over the prior art. This raises a suspicion that some of the methods are overspecialized or poorly tested. This work, inspired by the paper “Do we need hundreds of classifiers to solve real world classification problems?” by Ferández-Delgado et al. [27], strives to compare under “fair” conditions anomaly detectors to observe how the field has evolved in the last twenty years (the oldest compared detector [70] was published in 2000). Specifically, it investigates, if methods based on *deep* generative models offer a benefit over methods based on alternative paradigms (hereafter called *classical*).

Surely there already exist comparisons of anomaly detectors. Earlier surveys [68, 12, 30, 65] do not compare to deep generative methods, because they were not developed or sufficiently popular at that time. Contrary, the study in [44] contains a detailed description of deep models, but provides experiments only with the basic VAE and limited to specialized video datasets. Ref. [13] introduces a taxonomy of deep anomaly detection models but does not compare them experimentally. Other recent surveys [56, 50, 26, 88, 59] either ignore deep generative models altogether or describe them only theoretically, without making any experimental comparison. The most relevant prior art is [73], which tries to theoretically link deep and shallow techniques¹. But again,

an extensive experimental comparison of different generative models is missing. One would also expect papers introducing new methods to contain such a comparison. Some of them do [65], but generally, we have found comparisons limited (e.g. using a small number of datasets or methods) or flawed, which is elaborated below.

How does this paper avoid the aforementioned deficiencies? First, the comparison uses a large number of tabular datasets (40) prepared for anomaly detection [24, 65] and four image datasets popular in the evaluation of deep models. The datasets were chosen according to their appearance in the literature on anomaly detection, which implies that the methods are tested in an environment established in the community. We expect classical / deep methods to perform well on tabular / image datasets respectively. Second, eight classical methods in comparison serve as a baseline, over which we expect the state of the art deep methods should improve upon (latest compared method [89] was published in 2020). Third, all methods have been given the same conditions, which primarily means optimization of hyperparameters, as [80] has shown this to have a significant impact.

The saying “*the journey is more important than the goal*” is a cliché, but it is true in our endeavor for a fair comparison. We have uncovered many details and design decisions that have a profound effect on the outcome, yet our cross-checking with relevant publications revealed that their authors do not pay sufficient attention to them. Listing these details makes the second area of contributions of this paper, as we believe that by demonstrating and discussing their effects, some costly errors can be prevented in the future.

The list of contributions contains:

- 1) **The comparison** of classical and deep anomaly detectors on a large number of datasets helps to understand the limits of the state of the art and gives recommendation to practitioners.
- 2) **Sensitivity study** We have identified optimization of hyperparameters (including anomaly scores, ensembling, and kernels), evaluation protocol, and construction of datasets to be the main sources of variability.
- 3) **Evaluation pipeline** In line with reproducible research, we publish codes of the evaluation pipeline and compared methods. The pipeline automatically downloads datasets, splits them into training, validation, and testing, and calculates the performance metrics.

The paper is organized as follows. The next section briefly describes tested generative deep models and puts them into three main categories: generative flows, autoencoder-based models, and models based on the generative adversarial networks. Sec. III details the datasets, different approaches to selection of hyper-parameters, and other design decisions in the

All authors are with the Department of Computer Science, Faculty of Electrical Engineering, Czech Technical University, Prague, Czech Republic

¹The *shallow* techniques corresponds to those we call *classical*. We prefer the later terminology, as models based on random forests are in its essence deep, although they cannot capture semantic structure — a touted feature of deep models

experimental setup. Next, the experimental section discusses the experimental results and lessons we have learned. We summarize the paper with a recommendation to practitioners and our view of the weaknesses of the field.

II. COMPARED METHODS

This section briefly reviews deep generative models in order of exactness of calculation of likelihood. Therefore, it starts with flow models, continues with probabilistic (variational) autoencoders, where the prior art on the application in anomaly detection is rich, and finishes with two-stage models and generative adversarial networks, where the calculation of any score related to likelihood is dubious at best. We do not review classical methods here, as this has been done many times elsewhere. We list them in the relevant experimental section.

Before the description, we introduce a notation. Training samples, \mathbf{x} , are assumed to be i.i.d from the underlying probability distribution $p(\mathbf{x})$ defined on the input space \mathcal{X} . Following the conventional definition of an anomaly [6], each anomaly detection method is expected to provide a quantity (called score and denoted $s(\mathbf{x}')$) related to the probability a sample \mathbf{x}' being generated from $p(\mathbf{x})$. The score does not need to be a normalized distribution, as the threshold is typically determined as an empirical estimate of the quantile. Most functions in this section are assumed to have parameters optimized during training.

A. Normalizing flows

The name normalizing flows refers to methods relying on the change of variables formula

$$p(\mathbf{x}) = p(\mathbf{z})|\det J_f(\mathbf{z})|^{-1}, \mathbf{z} = f^{-1}(\mathbf{x}), \quad (1)$$

where $J_f(\mathbf{z})$ is Jacobi matrix of function f evaluated at \mathbf{z} . $p(\mathbf{z})$ is a known distribution of the latent variable \mathbf{z} from space \mathcal{Z} of the same dimension as \mathcal{X} .

Theoretical reviews [60, 47] require f to be invertible and both f and f^{-1} to be differentiable. Flow models therefore primarily differ in how they define the class of functions f , which ranges from simple affine transformations to solutions of ordinary differential equations. The expressive power comes from their composition as is usual in neural networks. In the comparison, we consider flows on tabular data only, for which we have implemented well known RealNVP [21] and MAF [61] flows alongside with a promising class of Sum Product Transform networks — SPTN [66] combining normalizing flows with a graphical model. The likelihood is used as a natural anomaly score.

Flow models have not yet enjoyed a lot of popularity in anomaly detection [93, 78, 20, 66] in comparison to autoencoders reviewed below. To us, this is surprising, since these methods can exactly calculate likelihood functions, which under a good fit is the ideal anomaly score. Meanwhile, the focus of the surrounding community is on the topic of *out of distribution detection* (OOD)² [57], which is very related to

²Out of distribution detection means identifying samples coming from a different dataset. For example, a model trained on MNIST / CIFAR10 should assign a low likelihood to samples from Fashion MNIST / SVHN respectively.

anomaly detection if not being equal. Ref. [16] suggests to use ensembles, while [71] recommends to convert the single-class problem to classification problems in the spirit of [84]. A deep investigation of OOD in [45], shows that with low-level features such as pixel intensities, flows tend to learn local models, i.e. according to taxonomy in [73] they fail to detect semantic anomalies.

B. Autoencoder-based models

Autoencoder-based models differ from flows by relaxing the exact mapping between $\mathbf{x} = f(\mathbf{z})$ (1) into a probability distribution $p_\theta(\mathbf{x}|\mathbf{z}) = \mathcal{N}(\boldsymbol{\mu}_\theta(\mathbf{z}), \text{diag}(\boldsymbol{\sigma}_\theta(\mathbf{z})))$,³ called *decoder*. The symbol θ denotes the trainable parameters of the decoder, e.g. weights of a neural network. The marginal likelihood is computed as

$$p(\mathbf{x}) = \int p_\theta(\mathbf{x}|\mathbf{z})p(\mathbf{z})d\mathbf{z}, \quad (2)$$

where $p(\mathbf{z})$ is a chosen prior probability distribution of the latent variable. This relaxation allows for more flexible models, e.g. using different dimension of \mathbf{x} and \mathbf{z} . However, training and evaluation of the model is more demanding since the marginal likelihood (2) is not available in closed form. Therefore [43] introduces *encoder* distribution $q_\phi(\mathbf{z}|\mathbf{x}) = \mathcal{N}(\boldsymbol{\mu}_\phi(\mathbf{x}), \text{diag}(\boldsymbol{\sigma}_\phi(\mathbf{x})))$ with parameters ϕ allowing approximation of Equation (2) as described below in Equation 3.

Various modifications of the original formulation have been proposed, giving rise to many specialized methods. Below we describe extensions in three blocks according to i) approximation of the likelihood (2) used for training, ii) approximations used for evaluating the anomaly score, and iii) various modifications that can be treated as hyperparameters.

a) *Training loss*: The original Variational Autoencoder [43] (VAE) proposes to replace (2) by the evidence lower bound [10] (ELBO)

$$\mathcal{L}_{\text{VAE}}(\theta, \phi) = -\mathbb{E}_{q_\phi(\mathbf{z}|\mathbf{x})} [\log p_\theta(\mathbf{x}|\mathbf{z})] + D_{KL}(q_\phi(\mathbf{z}|\mathbf{x})||p(\mathbf{z})), \quad (3)$$

which has an intuitive interpretation. The first term ensures that the output of the decoder is similar to the input \mathbf{x} and the second term is the Kullback-Leibler divergence (KLD) between the encoder distribution and the prior. If the model is well fit, samples from the prior projected by the decoder should have the same distribution as real data. In anomaly detection, KLD acts as a regularization term preventing overfitting. Models based on (3) will be referred to as the VAE family.

Asymmetry of the KL divergence motivated search for a more accurate metric. Ref. [85] proposes to replace KL by a Wasserstein divergence, yielding training loss function in the form:

$$\mathcal{L}_{\text{WAE}}(\theta, \phi) = -\mathbb{E}_{q_\phi} [\log p_\theta(\mathbf{x}|\mathbf{z})] + \lambda D(q_\phi(\mathbf{z}|\mathbf{x})||p(\mathbf{z})), \quad (4)$$

where $\lambda > 0$ is a scalar hyperparameter, an D is an arbitrary divergence. The most commonly used divergence is the kernelized maximum-mean-discrepancy (MMD) with kernel k evaluated using its unbiased empirical estimate on samples from

³Other forms of the distribution are possible, e.g. Bernoulli for scaled pixel intensities.

the encoding and prior distribution. It was reported that MMD performs well in matching high dimensional distributions [96] and also that it maximizes the mutual information between \mathbf{x} and \mathbf{z} , unlike KLD. Models based on (4) will be referred to as the WAE family.

An alternative choice of the divergence D in (4) proposed in [85] is the adversarial loss, which in combination with the Gaussian decoder coincides with the adversarial autoencoder [54]. This divergence introduces a third network $d_\psi(\mathbf{z}) : \mathcal{Z} \rightarrow [0, 1]$, called discriminator, trained to distinguish between samples from the prior $p(\mathbf{z})$ and samples \mathbf{x} projected by the encoder $q(\mathbf{z}|\mathbf{x})$. Every step of optimization separately updates the autoencoder and discriminator parts to minimize the loss functions

$$\mathcal{L}_{\text{AE}}(\theta, \phi) = -\mathbb{E}_{q_\phi(\mathbf{z}|\mathbf{x})} [\log p_\theta(\mathbf{x}|\mathbf{z})] - \lambda \log d_\psi(\mathbf{z}^q), \quad (5)$$

$$\mathcal{L}_{\text{D}}(\psi) = \log d_\psi(\mathbf{z}^p) + \log (1 - d_\psi(\mathbf{z}^q)), \quad (6)$$

respectively, where $\mathbf{z}^p \sim p(\mathbf{z})$, $\mathbf{z}^q \sim q_\phi(\mathbf{z}|\mathbf{x})$. Models trained with loss function (5) will be denoted as AAE.

b) Prior model: A common criticism of the VAE model is its use of the standard gaussian prior $p(\mathbf{z})$, which stimulates the distribution $q(\mathbf{z}|\mathbf{x})p(\mathbf{x})$ to have a single mode and therefore it is hard to fit data with a multi-modal latent distribution. Ref. [86] proposes a learnable multimodal *Vamp* prior realized as a mixture of K independent gaussian components. Vamp prior is compatible with AAE and WAE models since it does not have an analytical expression of KLD in (3). The mean values of components of the mixture are learned together with the parameters of the autoencoder. In the model selection below, the Vamp prior is considered as a binary hyperparameter with an additional parameter, K , specifying the number of components.

c) Anomaly Score: The likelihood function (2) also constitutes the ideal anomaly score. Some training losses such as ELBO (3) were designed as approximations of the likelihood and can thus be used as anomaly scores. However, this interpretation is not so clear for other training losses, i.e. (4), (5), hence their authors propose anomaly scores as part of the method. Nevertheless, many scores are interchangeable, giving rise to another degree of freedom (hyperparameter) for the use of autoencoders in anomaly detection. A common score is based on the first term in the loss i.e. a Monte Carlo estimate of the expectation of conditional log-likelihood over the encoder, yielding

$$s_{\text{rs}}(\mathbf{x}) = -\frac{1}{L} \sum_{l=1}^L \log p_\theta(\mathbf{x}|\mathbf{z}_l), \mathbf{z}_l \sim q_\phi(\mathbf{z}|\mathbf{x}). \quad (7)$$

This score, called sampled reconstruction error (abbreviated as rs), was shown in [92] to be more accurate than evaluating (2) by sampling \mathbf{z} from the prior $p(\mathbf{z})$. Further simplification is based on replacing samples from the encoder by its mean, yielding the common reconstruction error score (abbreviated as rm)

$$s_{\text{rm}}(\mathbf{x}) = -\log p_\theta(\mathbf{x}|\mu_\phi(\mathbf{x})) \quad (8)$$

The usage of (8) is justified by the assumption that taking the mean at the encoder should approximate (7) while having

lower computational demands. For adversarial autoencoders, the above simplifications can be combined with the discriminator score [77, 95],

$$s_a(\mathbf{x}) = \alpha s_{\text{rm}}(\mathbf{x}) + (1 - \alpha) d_\psi(\mu_\phi(\mathbf{x})), \alpha \in [0, 1]. \quad (9)$$

The above reconstruction-error based anomaly scores were criticized in [67] for not capturing the true data density $p(\mathbf{x})$. They propose a replacement based on the orthogonal decomposition of the data into $\mathbf{x} = \mathbf{x}^\perp + \mathbf{x}^\parallel$ where the \mathbf{x}^\parallel lies in the tangent space of to the manifold defined by the decoder. This allows to decompose the marginal likelihood into a product of two orthogonal parts

$$p(\mathbf{x}) \approx p(\mathbf{x}^\parallel) p(\mathbf{x}^\perp), \quad (10)$$

where $p(\mathbf{x}^\perp)$ is the reconstruction error, and $p(\mathbf{x}^\parallel)$ is obtained by transformation of variables (1). This score is below abbreviated as jc. The calculation of (10) is expensive, as it needs to compute the singular value decomposition of the Jacobian. For implementation details, see [67] or [82].

d) Other models and techniques: A plethora of models based on probabilistic autoencoders and specialized for anomaly detection was introduced in recent years, such as [99, 63, 92, 69, 15, 14]. Below, we list models included in the comparison and not described above.

The self-adversarial Variational Autoencoder (adVAE) [89] was included because it claims superiority over the state-of-the-art methods, such as VAE, DAGMM [99], WGAN-GP [34] or MO-GAAL [53] on tabular datasets. It augments the usual encoder-decoder pair with a transformer, whose goal is to simulate anomalies during training. We admit to being puzzled, as the model is trained only on normal data and there is no link between real and simulated anomalies. The sampled reconstruction is used as an anomaly score.

Despite its name, GANomaly [2, 1] is more related to adversarial autoencoders than to GANs. It consists of encoder-decoder-encoder with a discriminator, similar to an AAE. The anomaly score is the difference between latent representations of a sample after the first and second encoding. An upgrade to this model, skip-GANomaly [3], uses skip connections in a U-Net [72] type architecture. Here, the anomaly score is a combination of reconstruction error and feature-matching loss (see the next section on fmGAN). Although originally proposed only for use in images, we have implemented a variant for tabular data as well.

C. Generative adversarial networks

Generative adversarial networks [31] construct and train two networks: a generator $g_\phi(\mathbf{z}) : \mathcal{Z} \rightarrow \mathcal{X}$ and a discriminator $d_\psi(\mathbf{x}) : \mathcal{X} \rightarrow [0, 1]$ approximating the probability of \mathbf{x} being a sample from the data distribution rather than the generator. The generator aims to transform samples from $p(\mathbf{z}) = \mathcal{N}(\mathbf{0}, \mathbf{I})$ to \mathcal{X} such that they are indistinguishable from the real data. The discriminator and generator are trained as adversaries, hence the name. Formally, the optimization objectives are

$$\mathcal{L}_{\text{d}}(\psi) = \log d_\psi(\mathbf{x}) + \log (1 - d_\psi(g_\phi(\mathbf{z}))), \quad (11)$$

$$\mathcal{L}_{\text{g}}(\phi) = -\log d_\psi(g_\phi(\mathbf{z})), \quad (12)$$

where \mathcal{L}_d is maximized while \mathcal{L}_g is minimized, z is sampled from the prior and x from the training set. The optimization searches the saddle point of the two losses, which is difficult and notoriously unstable. Therefore a long series of work, e.g. [38], proposes improvements over the basic approach [31]. One of the approaches is based on the introduction of feature-matching loss [75]. We will denote the model trained with this loss as feature-matching GAN (fmGAN). In fmGAN training, the cost function of the generator is augmented with output of some intermediate (e.g. the penultimate) layer of the discriminator. Specifically, the generator is optimized as

$$\mathcal{L}_{\text{fm}}(\phi) = \alpha \mathcal{L}_g(\phi) + \|h_\psi(x) - h_\psi(g_\phi(z))\|^2, \quad (13)$$

where h_ψ is the output of the intermediate layer of the discriminator and z is a sample from $p(z)$. This feature-matching loss is used in AnoGAN for detection of anomalous objects in images, with hyperparameter α , which was zero in the original publication [75].

GANs are frequently augmented with a third model $q(z|x)$ [22] required to satisfy the cyclic property [98]. This makes the distinction between GANs and VAEs blurred, as demonstrated by using min-max (GAN-like) approximation of Wasserstein divergence in Wasserstein autoencoders, Sec. II-B. This makes it sometimes hard to assign a model to some class (for example GANomaly belongs according to us to probabilistic autoencoders).

Recall the role of the discriminator is to discriminate *generated* samples from *real* ones. Since the generator is trained to generate samples with a high discriminator score, it seems logical to use the discriminator to score anomalies

$$s_{\text{GAN}}(x) = 1 - d_\psi(x), \quad (14)$$

which is used e.g. in [53]. The common critique is that the discriminator was not trained to recognize an arbitrary distribution of the anomalies, but only that of the latent transformed by the generator. Thus it may fail to recognize anomalous samples of interest. AnoGAN [77] recognizes this flaw and proposes to augment the discriminator loss (13) for training and an iterative procedure that searches for the latent code z most likely to generate the tested sample to identify anomalous images. However, this procedure is computationally expensive. Its sequel, f(ast)AnoGAN [76], uses Wasserstein GAN with gradient penalization [34] to improve stability of stability and adds $q(z|x)$ to find z closest to given x in $q(z|x)$ faster. The anomaly score of fAnoGAN is a combination of discriminator score and feature-matching loss.

Multiple-Objective Generative Adversarial Active Learning (MOGAAL) [53], train k generators against a single discriminator on input data divided into k subsets. The usual discriminator score in Equation (14) is used to test new samples.

Other anomaly detection models derived from GAN certainly exist [95, 46, 64], however, it seems that autoencoder-based models are more popular for anomaly detection. Those included should be good representatives of SOTA, as we have selected those with good results in experimental comparisons.

D. Two-stage models

A recurring idea [25, 94, 74, 81] is to combine autoencoders with a secondary model acting on the latent space defined by the encoder. The rationale behind it is the encoder preserves semantic information of the sample and removes noise (e.g. background in images). It should therefore perform better in detecting semantic anomalies, but perform poorly on non-semantic ones. Additionally, reducing the size mitigates the curse of dimensionality [7], as high dimensions can be problematic for some models.

We are not aware of a general term for this approach. We use the term *two-stage models*, following [17], although [13] uses the term *deep hybrid models*. In [74], the model optimizes the projection of data (by virtue of NNs) to a new space, where they can be easily enclosed in a sphere of minimum radius. Approach presented in [81, 94] explicitly splits the creation of the detector into two parts. It first trains a VAE (and its variants) and then it fixes the encoder. The anomaly score is calculated by a kNN (in [81]) or by OC-SVM (in [94]) detectors in the latent space, obtained by projecting the sample by the fixed encoder. The two-stage models can be also viewed as a kNN with a trained metric or OC-SVM with a trained kernel.

E. Reducing hyper-parameter uncertainty by ensembles

Explicit notation of the hyperparameters, η , was not used in the above description. In reality, all estimates of the underlying probability defined above are conditioned on the chosen hyperparameter set, i.e. $p_\theta(x|\eta)$ ⁴ that may be significantly different for different values of the hyperparameter vector. Minimization of the influence of hyperparameters can be achieved by their estimation for the data and marginalization. Since this is typically intractable, a commonly used approach is to represent the hyperparameters by their samples $\{\eta_j\}_{j=1}^J$ and compute the marginal over them, using a Bayesian model average [37]

$$p(x) \approx \sum_{j=1}^J p(x|\eta_j, X) p(\eta_j|X). \quad (15)$$

Since the marginal likelihood $p(\eta_j|X)$ is often not available, a common approximation is to approximate (15) by unweighted average of selected hyperparameters [90], called (deep) ensembles. For anomaly detection, this approach corresponds to averaging of scores from multiple model instances, and some results are reported in [16, 57].

III. EXPERIMENTAL SETUP

A. Datasets

The experiments used two types of datasets: *tabular* and *image*. The idea behind this choice is that the former are popular in the evaluation of *classical* methods, where anomalies should have statistical sense and should be located in areas of low likelihood of normal class, while the latter is favored in the evaluation of *deep* methods, where anomalies

⁴If θ is the set of trained parameters, then it probably depends on the chosen hyperparameters, e.g. the number of hidden units dictates the dimensionality of θ . But for brevity, this dependency is omitted here.

have semantical meaning.⁵ Therefore, we expect the methods to be tuned to corresponding datasets, and having both allows the assertion of weaknesses. The choice of datasets (mainly the tabular ones), was guided by two criteria: first, they ought to be publicly available and second, they should appear in surveys or in articles presenting new methods. In total, we have collected 40 tabular datasets, the majority of which came from the UCI repository [23]. With the exception of ANNThyroid, Arrhythmia, HAR, HTRU2, KDD Cup 99 small, Spambase, Mammography, and Seismic, where the anomaly class has a clear semantic meaning (security incident or disease), we have followed the technique of [24] for creating datasets for anomaly detection tasks. More precisely, we have used only "easy" and "medium" anomalies, as "hard" and "very hard" are not really anomalies in the sense of being clearly statistically distinct from the normal class. Prior to model training, features on tabular datasets were normalized to have zero mean and unit variance. Further details of the datasets are provided in Tab. I.

The number of datasets used for evaluation of deep models is limited, as most works use one of the four popular image datasets: MNIST [51], FashionMNIST [91], CIFAR10 [49], and SVHN2 [58], needless to say, the prior art does not provide consensus on what is considered an anomalous class. In this work, we have considered all of them in two different settings, which are described in detail below. No preprocessing has been applied prior to training, with the exception of linear extrapolation, which was needed to fit the architecture of some of the methods, namely GANomaly [2]. Basic statistics on image datasets are shown in table Tab. II.

B. Data splits and experiment repetitions

It should be a gold standard that the experiments are repeated on different splits of data to training, validation, and testing subsets, especially if the datasets are small. However, in most of the reviewed recent papers [53, 89, 77, 2, 64], this procedure was not mentioned with an exception of [74]. Therefore, our comparison fills this gap. The experiments on tabular data were repeated five times with different splits. On image data, the results are averaged over 10 anomaly classes instead.

Specifically, in each repetition (five in total) of an experiment on tabular data, the *normal data* in each dataset were randomly split in 60%/20%/20% ratios to train/validation/test subsets, respectively. *Anomalous data* were split such that 50% were in the validation part and 50% in the testing part, which means the training subset has not contained anomalous samples.⁶ This experimental repetition enables a more robust and fair validation and hyperparameter optimization, which will be discussed in the following text. However, different choice of hyperparameters may arise in the case of contaminated

⁵Semantical anomalies do not have to be in areas of a low likelihood of the pixel space of the normal class, since there can be a huge contribution of noise (background).

⁶A training set without any anomalies is in practice very optimistic, but this decision removes another degree of freedom from the evaluation for the sake of clarity of results.

dataset	alias	dim	anom	normal
ANNthyroid	ann	21	534	6665
Arrhythmia	arr	275	206	245
HAR	har	561	1944	8355
HTRU2	htr	8	1638	16257
KDD99 (10%)	kdd	118	396742	97276
Mammography	mam	6	260	10921
Seismic	sei	24	170	2412
Spambase	spm	57	1812	2786
Abalone	aba	10	50	2151
Blood Transfusion	blt	4	16	382
Breast Cancer Wisconsin	bcw	30	206	356
Breast Tissue	bts	9	22	65
Cardiotocography	crd	27	228	1830
Ecoli	eco	7	108	205
Glass	gls	10	94	112
Haberman	hab	3	14	225
Ionosphere	ion	33	122	225
Iris	irs	4	46	100
Isolet	iso	617	3300	4496
Letter Recognition	ltr	617	3600	4196
Libras	lbr	90	142	215
Magic Telescope	mgc	10	3882	12331
Miniboone	mnb	50	23922	93565
Multiple Features	mlt	649	800	1200
PageBlocks	pgb	10	384	4911
Parkinsons	prk	22	44	146
Pendigits	pen	16	5384	5537
Pima Indians	pim	8	176	500
Sonar	snr	60	96	110
Spect Heart	sph	44	52	211
Statlog Satimage	sat	36	2630	3592
Statlog Segment	seg	18	938	1320
Statlog Shuttle	sht	8	28	57767
Statlog Vehicle	vhc	18	132	627
Synthetic Control Chart	scc	60	200	400
Wall Following Robot	wrb	24	2220	2921
Waveform-1	wf1	21	1482	3302
Waveform-2	wf2	21	1472	3302
Wine	wne	13	70	106
Yeast	yst	8	390	751

TABLE I: Basic statistics of the tabular datasets.

training, as good performance of the orthogonal score has been observed for contaminated training in [83].

All used image datasets contain 10 classes. While on tabular data, the anomalous class is either given or converted from multi-class to binary following [24], on image datasets the common practice is to either train on one class and treat the complement as anomalous (hereafter called *leave-one-in*) [64, 67, 74], or vice versa train on nine classes and use the remaining one as anomalous (hereafter called *leave-one-out* [55]). In the case of image datasets, we have substituted repetitions of an experiment by class-splits, since the number of samples is large and our initial experiments (see supplementary Tab. C.1) have not exhibited a large variation between different repetitions. As will be shown below, the choice between *leave-one-in* and *leave-one-out* has a profound effect on results.

C. Notes on implementation of models

As mentioned in the introduction, we have compared *deep* methods to *classical* ones serving as an etalon. Classical methods included ABOD [48], HBOS [29], LODA [65], LOF [11], IsolationForest [52], OC-SVM [79], PIDForest [32],

dataset	alias	dim	anom	normal
CIFAR10	cifar10	32x32x3	6000	54000
FashionMNIST	fmnist	28x28x1	7000	63000
MNIST	mnist	28x28x1	6312	63686
SVHN2	svhn2	32x32x3	18960	80327

TABLE II: Basic statistics of image datasets where one of the 10 classes is considered anomalous — in the text referred to as *leave-one-out* setting

model	acronym	model	acronym
AAE	aae	MAF	maf
ABOD	abod	MOGAAL	mgal
adVAE	avae	OC-SVM	osvm
DeepSVDD	dsvd	OC-SVM _{RBF}	orbf
fAnoGAN	fano	PidForest	pidf
fmGAN	fmgn	RealNVP	rnvp
GAN	gan	skipGANomaly	skip
GANomaly	gano	SPTN	sptn
HBOS	hbos	VAE-kNN	vae
IsolationForest	if	VAE-OC-SVM	vaeo
kNN	knn	VAE	vae
LODA	loda	WAE	wae

TABLE III: Overview of model acronyms.

and kNN [70]. For ABOD, HBOS, and LODA, we have used implementation from pyOD library [97]), for LOF, IsolationForest, and OC-SVM we used implementation from scikit-learn [62], and last but not least we have used our own implementation of kNN.

Since image datasets are typically much larger than tabular, an ensemble of OC-SVM models was trained on subsets of image data, see Sec. E.

To ensure consistency among deep models, we implemented all methods except the MOGAAL⁷ ourselves using the Flux [39] framework in Julia [9] language. Apart from the models mentioned in Sec. II, we have also implemented the state-of-the-art DeepSVDD [74] both for image and tabular data.

We emphasize that while implementing models, we have carefully compared our implementations to the reference where possible and (or) verified that our experimental results are similar to those provided in the corresponding publication.

Neural networks were trained with the ADAM [41] optimizer with early stopping measuring the continued decrease of loss on the validation dataset. As stated above, models with convolutional layers were used on image data, while dense layers were used on tabular data. More implementation details are in the supplementary materials Sec. E. The implementation code in the form of a Julia package can be found at <https://github.com/aicenter/GenerativeAD.jl>.

D. Hyperparameters and their optimization

Properly exploring the space of hyperparameters of all models is paramount to achieving fair and comparable experimental comparison, yet this is often superficially treated. Researchers often use *default* or *recommended* values ignoring

they are sub-optimal on datasets they use in their comparison. A nice demonstration of this are conflicting results of the MOGAAL [53] in the original publication and in [89]. A prototypical example is OC-SVM, which is typically used with Gaussian kernel and with ν set to some default value, for example 0.05 [65], but can achieve better results with different kernels. The choice of hyperparameters in anomaly detection is everything but easy. But this means that the experimental settings should be set up such that all methods have been optimized equally. We conjecture that recommended and default values of hyperparameters are strongly correlated with the choice of evaluation datasets in the publications that recommend them.

This work adopts the approach from [80], where hyperparameters are chosen using labeled samples in validation sets, which is standard in supervised learning. It is also supported by our industrial experience, where examples of anomalies are almost always available, although the price for their acquisition can be high. Since the number of anomalies⁸ in the validation set influences the quality of selected hyperparameters, Ref. [80] proposes to visualize this relation as a trend in a graph.⁹

The search for hyperparameters uses random sampling on predefined grid¹⁰, which is frequently more efficient than grid search [8] and more flexible. For each model, dataset, and repetition, we have sampled 100 configurations from corresponding sets (see Tab. A.1–A.3) and trained the models with them. In order to keep the neural-network based models fixed across the repetitions on a single dataset, for each hyperparameter configuration we have also sampled a random seed that was used to initialize the network weights. To prevent running the search in expensive methods forever, there was a hard deadline of 24 hours in which the training of a single configuration for a given number of repetitions/classes should be finished. This automatically penalizes complicated models. The number of trained configurations for each model is in supplementary materials in Tab. B.2, B.3, C.7 and C.8.

Encoders for the two-stage models were selected from models performing best in terms of validation AUC or reconstruction error on the validation set. The second-stage models (kNN and OC-SVM) used hyperparameters sampled from Tab. A.1. Due to a deeper investigation of models with many variants, there were sometimes more than 100 available configurations for a given model. In these cases, the best configuration was selected from a random subset of size 100, which ensures these models do not get an unfair advantage.

For choosing the best models into ensembles, we employed only performance metrics on validation data such as AUC or TPR at 5% of FPR, as the WAIC score from [16] is available only for models with exact or approximate likelihood. We have also experimented with different fixed sizes of ensembles —

⁸It is assumed all anomalies in validation set are known.

⁹In some application scenarios the examples of anomalies are not available at all. In this case, one has to resort to methods that can tune on normal samples only, such as flow models or LODA. Since most methods in this comparison do not have this feature, this approach is not pursued here.

¹⁰which allows the construction of sections through the space for sensitivity studies

⁷The pyOD implementation was used.

either top 10 or top 5.

In total, we have trained 856,464 model instances in 6035 CPU days, evaluated 2,670,726 different scoring functions in 1697 CPU days, and created 6.4TB of experimental data.

E. Selecting hyperparameters in repeated experiments

In the prior art, we have identified two approaches to the selection of hyperparameters when experiments are repeated.

First, which is called *mean* in this text, a model has the same configuration of hyperparameters on all repetitions of the experiment (naturally, for each dataset the configuration is different). The selected configuration is the one achieving the best average performance on the validation sets across all five repetitions. We believe this to be more common [74], although it is difficult to confirm, as many papers do not share this detail.

Second, which is called here *max*, each repetition of the experiment (on the same dataset) uses a different configuration corresponding to the best one on its validation set. This method is to our knowledge used rarely [66], but the argument for it is that it better uncovers the true potential of methods. However, the selection is subjected to more noise, especially if a fewer number of anomalies is known.¹¹

IV. EXPERIMENTAL RESULTS

Unless said otherwise, experimental results presented below are estimates of the area under the ROC curve estimated on the testing set and averaged over five repetitions (tabular datasets) or 10 anomalous classes (image datasets with one class left as anomalous — leave-one-out). When ranks are reported, they are calculated by ordering methods on each dataset and calculating average across them (as recommended in [19]). Hyperparameters are selected using the *mean* protocol on tabular data, and the *max* protocol on image data, because the split by classes constitutes different anomaly detection problems. Variational auto-encoders use sampled reconstruction error (7).

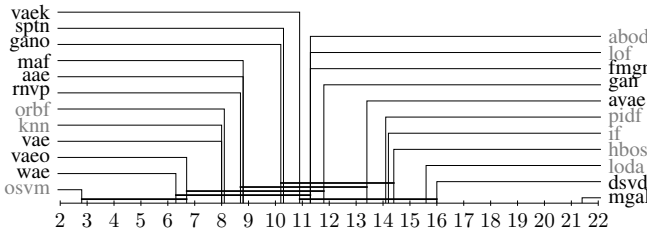


Fig. 1: Critical difference diagram of models ranked via AUC on the tabular data. Models whose performance is statistically indistinguishable have difference of ranks under the critical value of the Nemenyi test $CD_{0.1}(23, 40) = 5.15$ and are joined by a horizontal band.

¹¹The number of known anomalies in the validation set is limited per repetition of the experiment. This means that the *mean* approach effectively uses more known anomalies to select the hyperparameters than the *max* approach. We hope that this discrepancy will not influence the results negatively in favor of the *mean* approach.

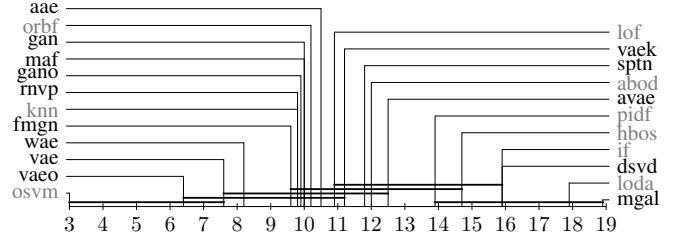


Fig. 2: Critical difference diagram of models ranked via the TPR@5 criteria on the tabular data.

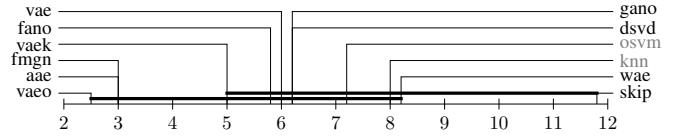


Fig. 3: Critical difference diagram of models ranked via AUC on image data. $CD_{0.1}(12, 4) = 7.72$.

A. Comparison of detectors

The results of experimental comparison on tabular and image data, presented in the form of Critical difference diagrams (CDD) as recommended by Demšar [19], are in Fig. 1 and C.1. The acronyms used in the figures are summarized in Tab. III. Figures show an average rank of detectors across the datasets together with a confidence band that indicates that a statistical test cannot reject the hypothesis that detectors performs the same. The underlying test AUC values with average ranks are shown in Tables IV and VI for the image data.

On *tabular data*, OC-SVM works the best and it is *statistically better* than almost all detectors except WAE and VAE combined with OC-SVM. This very surprising phenomenon is studied in detail in Sec. IV-C2. The first 13 places (roughly one half) belong to models that can be divided into three groups: (i) OC-SVM and its variants, which estimates a density level of a distribution; (ii) flow models and kNN which estimates the pdf (kNN un-normalized); (iii) and variants of auto-encoders, where reconstruction error is related to pdf as explained in [82]. A detailed discussion of auto-encoders is below in Sec. IV-C1. The position of two-stage models might be surprising, yet explainable if the encoder-decoder identified the manifold of data. We believe that the models in the lower half of the scale are not statistically well-founded for the problems (GANs, as mentioned in Sec. II-C) or they are not sufficiently flexible (LODA, HBOS, IF, PIDF). We cannot explain the poor performance of MOGAAL and adVAE¹² and we attribute it to different experimental environment.

Differences in mean ranks of many models in Fig. 1 are statistically insignificant at level $p = 0.1$, which is disappointing. Assuming the ranks remain the same, another 47 datasets would be needed to make the difference between OC-SVM and WAE statistically significant.

¹²We have contacted the author of pyOD from wherein we took the implementation of MOGAAL and we were assured that his implementation is a copy of that provided by the authors. Therefore, we consider the implementation to be correct.

While the AUC is undoubtedly the gold-standard metric of the field, practitioners are often more interested in behavior on low-positive rates. Fig. 2 shows the same CDD plot with detectors ranked by the true positive rate estimated at 5% false positive rate, TPR@FPR ,¹³ (table with the underlying values is provided in supplementary in Tab. B.1). We can see changes in ranks, but the overall tendency of OC-SVM and autoencoders dominating the results remains, despite the improved performance of some GAN models.

Image data: While tabular datasets contain *statistical anomalies* (they occupy an area of low likelihood), it is believed image data to contain *semantic anomalies* (see [73]. Fig. C.1 shows CDD diagram with ranks calculated using the AUC with test set following *leave-one-out* protocol. Tab. VI contains the average AUC per dataset and results per fold can be found in Supplementary in Tab. C.5. By no surprise, OC-SVM ranks poorly, but its combination with variational auto-encoders in a two-stage model performs the best. We believe this to be caused by the VAE extracting semantic description of scenes, which is then well modeled by OC-SVM. Notice that many recently proposed methods, namely skip-GANomaly [3], DeepSVDD [74], GANomaly [2] perform inferior to the vanilla VAE. We attribute this to insufficient tuning of hyperparameters and chosen *leave-one-out* protocol, which is according to our experiments harder than the widely used *leave-one-in* as demonstrated by higher AUC values in Tab. VII. The statistical tests on image datasets are inconclusive due to their small number.

We notice that the experimental results on the image dataset are generally poor, as the AUC of the best model (feature-matching GAN) on CIFAR10 is 0.7 and similarly on SVHN2, where the best model (again feature-matching GAN) achieved 0.58, which is not that far from random guessing. The only dataset, where the anomaly detection works nicely is MNIST, where differences among numbers are significant. This indicates that the models fail to learn or identify the semantic information, or they consider different semantic information anomalous and they should be told *which* semantic aspect of an image should be considered as an anomaly, as for example blurred images might be anomalous as well.¹⁴

The AUCs of the same models estimated by the *leave-one-in* protocol (Tab. VII) gives a more optimistic view on the problem, as the best AUC on SVHN2 improves from 0.58 to 0.73 and similar improvement can be seen on Fashion MNIST and on MNIST. Modeling a single class is clearly much easier than nine-classes, as a single class can have a uniform background or low variance of object appearances. We have verified this claim by creating a detector counting number of blue pixels. This detector was on par with others on the problem, where the normal class label was "airplane". Details of this experiment are in Supplementary in Sec. C. It also shows top outliers and inliers of some methods under the *leave-one-in* protocol, which supports our hypothesis that the

leave-one-in protocol does not measure the quality of detecting semantic anomalies. Two stage combination of VAE and kNN ranks the best, with numerous other methods offering almost the same performance — VAE, AAE, and WAE. Interestingly, fmGAN outperforms the rest on color images (SVHN2 and CIFAR10 datasets) but does not perform so well on black-and-white.

B. Protocols

Throughout the manuscript, we emphasize that small changes in the evaluation protocol have a profound effect on the outcome. In Sec. III-E we described two approaches to selection of hyperparameters — *mean* and *max* — differing in whether the hyperparameters are shared across experimental repetitions (folds) or optimized per fold. Tab. V shows the difference in the approaches where the rank of some methods can change up to two points (MOGAAL), and the average AUC changes as well.

Similarly, the same table shows that a similar difference can be observed when only a single repetition of the experiment is done (see for example change of ranks AAE, OC-SVM, LOF, and fmGAN in seeds 1 and 5). It is surprising to us to see publications mentioned in Sec. III-B are not adhering to this gold standard of the community.

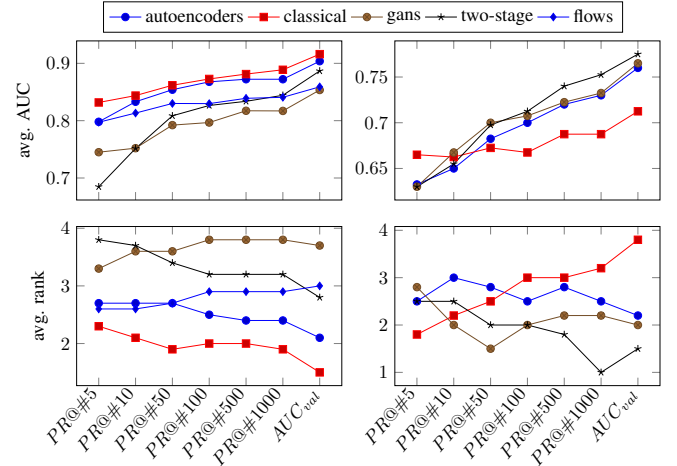


Fig. 4: Sensitivity of methods to the number of anomalies available for hyperparameter selection visualized in terms of the achieved AUC (top row) and their average rank (bottom row) for both the tabular (left column) and the image datasets (right column). Each point represents the best models of a certain category under given selection criterion.

C. Optimization of hyperparameters

The process of selecting hyperparameters described in Sec. III-D depends on the availability of examples of anomalies in the validation sets (recall that it is assumed that the validation dataset does not contain unknown anomalous samples, i.e. are not dirty). Fig. 4 displays the influence of the number of anomalous samples in the validation set on the quality of the selected model. Specifically, the number of

¹³Hyperparameters were selected according to the same criterion measured on validation set.

¹⁴While we stay away from philosophical aspects, the semantic anomaly detection might be replaced by a one / few-shot learning, as in all our experiment we needed few anomalies for selection of hyperparameters.

TABLE IV: Performance of models on tabular datasets with hyperparameter selection using the *mean* aggregation on the validation data, reported in the AUC metric on the test data, averaged over 5 folds. σ_1 is the standard deviation for the best model over the folds, while σ_{10} is the average standard deviation of the best 10 models. The final row contains the average model rank.

TABLE V: Comparison of average ranks in the AUC and TPR@5 metrics using both evaluation protocols together with examples of one repetition results on seed 1 and 5.

TABLE VI: Average AUC values of methods tested on the image data using the *leave-one-out* strategy. Reported are the AUC values on the test dataset, averaged over 10 anomaly classes. σ_1 is the standard deviation for the best model over the 10 folds, while σ_{10} is the average standard deviation of the best 10 models.

TABLE VII: Average AUC values of methods tested on the image data using the *leave-one-in* strategy. Reported are the AUC values on the test dataset, averaged over 10 anomaly classes. σ_1 is the standard deviation for the best model over the folds, while σ_{10} is the average standard deviation of the best 10 models.

normal samples was kept the same, and only the number of anomalous ones used to calculate the PR@ $\#n$ score (precision at n most anomalous samples) for selecting the best model and hyper-parameters was varied. To prevent visual clutter, models are grouped by their corresponding category which itself is thought of as a method with heterogeneous hyperparameters, one of which is the model's name. This setting also allows to show the maximum potential of each category as the evaluation protocol's can choose the best representatives for each dataset separately. We observe that with the increasing number of anomalous samples the quality of the selected model improves, which is expected, but on tabular data, the relative performance (ranks) changes only a bit at the beginning, and especially the flow models are better than autoencoders for a limited number of validation samples. The situation on image data is more erratic, which we attribute to the generally poor performance of methods and therefore to higher noise in the evaluation. However, the main differences can be observed again for low number of samples in the validation set, in which case, the classical method outperforms the recent methods.

1) *Sensitivity Analysis of VAE*: In Sec. II-B, the variability in VAE was divided along three dimensions: approximation of the likelihood in training (loss function), the richness of latent prior, and the anomaly score. Additional degrees of freedom include the parametrization of variance of $p_\theta(\mathbf{x}|\mathbf{z})$, which could be either fixed (called VAE-constant), used in [94, 89, 1], scalar (called VAE-scalar), or full diagonal (called VAE-diagonal), used in [4, 92, 95]. In the experiments, all three

variations were tested on tabular data, though on image data the full diagonal was skipped due to computational constraints (and in line with the prior art, where only fixed variance is used).

The overall comparison in Tab. IV revealed that WAE and vanilla VAE variants perform best, while the other degrees of freedom, namely richness of prior, and parametrization of variance were treated as hyperparameters (anomaly score in Tab. IV was fixed to be the resampled reconstruction error). Fig. 5 fills this gap by showing the distribution of ranks over tabular datasets for different variants of VAE including GANomaly and adVAE.

First, notice that the spread of the method's ranks over various datasets is significant, as even ranks of the best methods vary from 3 to 15. This means that the conclusions below need to be taken with a grain of salt, as the experimental results are extremely noisy.¹⁵

The ELBO-based score, -el, together with the orthogonal decomposition of the likelihood [67], -jc, does not perform well. A sampled reconstruction error (an MC estimate of (7)), -rs, almost always performs better than the usual reconstruction error, -rm, calculated according to (8). This demonstrates the common approach of replacing the mean of the decoder with that of the encoder is inferior but computationally cheaper (see Tab. VIII with prediction times). The discriminator score (14), -di, of AAE (an autoencoder combined with GAN) seems to be also on par with the MC estimate (7).

From the same figure, we also conclude that the models modelling full diagonal in $p_\theta(\mathbf{x}|\mathbf{z})$, -d-, seem to be better than the scalar, -s-, or constant, -c-, variants. This result is important, as many comparisons in the prior art use the VAE-constant, despite the version with full diagonal being discussed in the original publication [43].

The rich prior distribution on the latent space proposed in [86], VAMP, -v-, does not seem to give an advantage in the anomaly detection except in the AAE. Similarly, recent variants adVAE and GANomaly do not seem to work well on the tabular data, but true to their authors, they have never been evaluated on them.

2) *Sensitivity study of OC-SVM*: The experimental comparison on the tabular data was dominated by the OC-SVM

¹⁵A particularly interesting source of noise is the extrapolation of manifold outside data. This causes reconstruction error to be low in parts of the space, where no data has been observed. Since this area is around a set of measure zero if it does not hit by accident anomalies, which would make them undetectable, the reconstruction error works well. This problem is described in detail in [83].

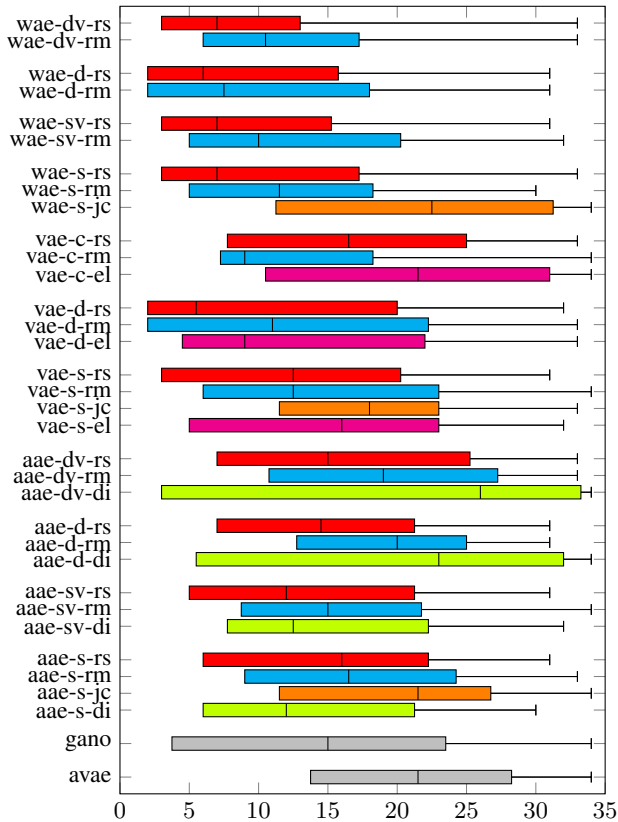


Fig. 5: Sensitivity study of various variants of autoencoder-based methods displayed in the form of boxplots of their ranks in the AUC metric achieved on the tabular datasets. The first three letters of the method’s name denote the training loss. Models with the -d- middle part estimate full diagonal of the decoder variance, -s- estimate only a scalar, and -c- use a fixed scalar variance as a hyperparameter. All variants are using the standard Gaussian latent model. Models using the VampPrior are denoted by extending the decoder variance symbol by the letter v-, i.e. -dv-, -sv-, -cv-. The last part of the name denotes score, -rs stands for the sampled rec. probability (7) with $L = 100$, -rm for (8), -el for the ELBO (3) composed of -rs and KLD, -jc for (10), -di for (14).

	vae-s-rs	vae-d-rs	vae-s-rm	vae-d-rm	vae-d-jc
\bar{t}_{pred} [s]	12.10	18.51	0.11	0.15	57.31

TABLE VIII: Average prediction times on the tabular datasets for different combinations of VAE scores and decoder variance estimations. The -d- part stands for model with an estimate of the full diagonal of the decoder variance, -s- is a scalar estimate. Sampled reconstruction error (7) is denoted as -rs, -rm is the anomaly score (8) and -jc is (10).

model, which is in sharp contrast to many prior experimental comparisons [30, 14, 18, 32, 40, 89]. The search for the culprit found it to be the hyperparameter selection. This study has varied the ν parameter, kernels, and their parameters, which is much more than the most prior art does, which is fixing the kernel to RBF and tests few values of its width γ and ν . Inclusion of other kernels into the search for hyperparameters seems to be the major source of improvement. The OC-SVM restricted to use only the RBF kernel and $\nu = 0.5$, denoted in Tab. IV as **orbf**, performs significantly worse.¹⁶ In the above experiments, the sigmoid kernel was the optimal choice for 23 datasets, while the RBF kernel only for 13. A good performance of the OC-SVM should not be surprising, as it converges to the true density level set [87]. Ref. [30] mentions that setting $\nu = 0.5$ provides universally good results, which may be the reason why many authors do not tune it, and also it contrasts with theory, according to which it should be set to much lower values ($\nu = 0.05$).

D. Ensembles

The benefits of ensembles in prior art seem to be mixed. While [16] claims that a combination of VAE or GAN ensembles using WAIC might be useful, Ref. [57] claims a negligible effect. In our experiments, we have used ensembles as a way to reduce uncertainty in hyperparameters [90], meaning that unlike in [16], models in ensembles were of a single type differing only in architecture.

The effect of ensembles on average AUC was overall zero, sometimes even negative. Exceptions are methods based on GANs featuring improvements by 0.02 in average AUC (Tables with results are in supplementary materials Sec. D). These findings are on par with those in [57].

E. Recommendation for practitioners

Practitioners ask for fast and accurate algorithms, but these two features rarely go hand in hand, and a decision on a trade-off has to be made. Interesting methods lie on the Pareto frontier, as in absence of external factor, rationally behaving practitioner does not have a motivation to choose a different model.

Fig. 6-right shows trade-off between accuracy and training time, where the absolute numbers were replaced by average ranks for robustness. The Pareto frontier contains a single method, which is OC-SVM. This is rather surprising, as its training time is known to scale poorly (quadratically) with respect to the number of samples, but it might be caused by most of the tabular datasets being small. The training times of neighbor based methods, kNN and LOF, are non-zero due to efficient structure for fast nearest neighbor search being built during training.

Fig. 6-left shows a similar trade-off between accuracy and testing (inference) time. OC-SVM is still on the Pareto frontier, but it is expensive, as the complexity grows linearly with respect to the number of samples. VAE combined with OC-SVM is there as well, and the faster testing time suggests

¹⁶The width of the kernel was still optimized.

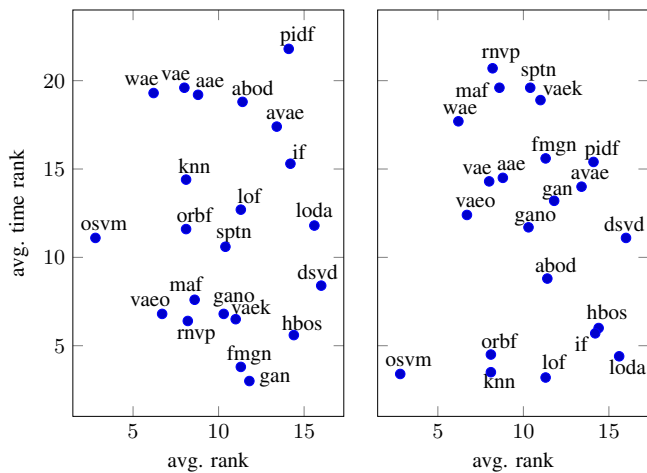


Fig. 6: Scatter-plots of the average rank in the AUC metric on the tabular data versus average rank of the computational complexity of the displayed methods measured via the prediction time (left) and the training time (right). MO-GAAL has been omitted from the figures, as its performance positioned it too far to the right with the training time rank of 17.1 and the prediction time rank of 11.9.

that encoding makes the problem simpler requiring a smaller number of support vectors. Finally, the Pareto frontier contains GAN and its feature-matching variants, which have fast inference but are inaccurate. A rather surprising is the computational complexity of VAE and its variance, which is caused by the complexity of sampled reconstruction error score (7) (see Tab. VIII with inference times).

A practitioner might also desire a method robust with respect to poor choice of hyper-parameters. That is demonstrated in Tables IV, VI, and VII showing the mean variance of the best model over experiment repetitions σ_1 as well as the mean AUC variance for the 10 best models σ_{10} . In general, deep models have a higher variance, probably due to the large number of hyperparameters and stochasticity involved in their initialization and training via batched gradient optimization. The values of σ_{10} hint at the potential cost of hyperparameter optimization — with lower values, one is more likely to train a well-performing model in fewer attempts. In this respect, GAN-based models seem to be the least robust, which is in line with [18] stating that GANs are not directly optimized for anomaly detection. The same effect is observed on image datasets (Tab. VI), where fmGAN performs very well, but exhibits the highest variance in performance as evidenced by σ_{10} .

V. CONCLUSION

The presented extensive comparison of anomaly detection methods based on deep generative methods, namely variants of variational autoencoders and generative adversarial networks with methods based on alternative paradigms (Support vector machines, random forests, histogram and distance-based methods) brought a surprising result. On the tabular datasets, the one-class support vector machines, one of the oldest

compared methods, dominated all the other methods by a large margin. A careful search for the culprit has revealed that unlike comparisons in the prior art, we have tried other kernels than RBF. On image datasets, the overall best model was a combination of the variational autoencoder with one-class SVM, although feature-matching GAN was very good as well.

Unlike majority of the prior art, we have also reverted the usual protocol of learning on a single class and deeming the rest anomalous to learning on nine classes and using the remaining one as anomalous. This change has revealed that although it was generally believed that deep generative anomaly detectors model semantic information, they do not. We have shown that they are fooled by a typical background and in some cases perform similarly to a detector counting the number of pixels of a particular color. This raises the question of whether the prevalent approach of not using any labeled examples of anomalies makes sense in these challenging domains. How can the algorithm learn that we are interested in images containing foreign objects and not in blurred images?

The comparison is not aimed only at researchers, but also at practitioners desiring accurate methods with low computational complexity. Therefore, we visualize these trade-offs, such that they can choose models on the Pareto frontier, which a rational practitioner should do.

ACKNOWLEDGMENTS

Support of grants GACR GA18-21409S, MSMT CZ.02.1.01/0.0/0.0/16_019/0000765 and SGS18/188/OHK4/3T/14 is gratefully acknowledged.

REFERENCES

- [1] Hyojung Ahn, Dawoon Jung, and Han-Lim Choi. Deep generative models-based anomaly detection for spacecraft control systems. *Sensors*, 20:1991, 04 2020.
- [2] Samet Akcay, Amir Atapour-Abarghouei, and Toby P. Breckon. Ganomaly: Semi-supervised anomaly detection via adversarial training. In *Asian conference on computer vision*, pages 622–637. Springer, 2018.
- [3] Samet Akcay, Amir Atapour-Abarghouei, and Toby P. Breckon. Skip-ganomaly: Skip connected and adversarially trained encoder-decoder anomaly detection. In *2019 International Joint Conference on Neural Networks (IJCNN)*, pages 1–8. IEEE, 2019.
- [4] Jinwon An and Sungzoon Cho. Variational autoencoder based anomaly detection using reconstruction probability. *Special Lecture on IE*, 2(1):1–18, 2015.
- [5] Martin Arjovsky, Soumith Chintala, and Léon Bottou. Wasserstein gan. *arXiv:1701.07875 [stat]*, 2017.
- [6] Vic Barnett and Toby Lewis. *Outliers in statistical data*. Wiley, 1974.
- [7] Richard E Bellman. *Adaptive control processes*. Princeton University Press, 1961.
- [8] James Bergstra and Yoshua Bengio. Random search for hyper-parameter optimization. *The Journal of Machine Learning Research*, 13(1):281–305, 2012.

- [9] Jeff Bezanson, Alan Edelman, Stefan Karpinski, and Viral B Shah. Julia: A fresh approach to numerical computing. *SIAM Review*, 59(1):65–98, 2017.
- [10] Christopher M Bishop. *Pattern recognition and machine learning*. springer, 2006.
- [11] Markus M Breunig, Hans-Peter Kriegel, Raymond T Ng, and Jörg Sander. Lof: identifying density-based local outliers. In *Proceedings of the 2000 ACM SIGMOD international conference on Management of data*, pages 93–104, 2000.
- [12] Guilherme O Campos, Arthur Zimek, Jörg Sander, Ricardo JGB Campello, Barbora Micenkova, Erich Schubert, Ira Assent, and Michael E Houle. On the evaluation of unsupervised outlier detection: measures, datasets, and an empirical study. *Data Mining and Knowledge Discovery*, 30(4):891–927, 2016.
- [13] Raghavendra Chalapathy and Sanjay Chawla. Deep learning for anomaly detection: A survey. *arXiv:1901.03407 [cs]*, 2019.
- [14] Raghavendra Chalapathy, Edward Toth, and Sanjay Chawla. Group Anomaly Detection using Deep Generative Models. *arXiv:1804.04876 [cs]*, April 2018.
- [15] Xiaoran Chen and Ender Konukoglu. Unsupervised detection of lesions in brain mri using constrained adversarial auto-encoders. *arXiv:1806.04972 [cs]*, 2018.
- [16] Hyunsun Choi, Eric Jang, and Alexander A. Alemi. WAIC, but Why? Generative Ensembles for Robust Anomaly Detection. *arXiv:1810.01392 [cs, stat]*, May 2019.
- [17] Bin Dai and David Wipf. Diagnosing and enhancing vae models. *arXiv:1903.05789 [cs]*, 2019.
- [18] Lucas Deecke, Robert Vandermeulen, Lukas Ruff, Stephan Mandt, and Marius Kloft. Image anomaly detection with generative adversarial networks. In *Joint european conference on machine learning and knowledge discovery in databases*, pages 3–17. Springer, 2018.
- [19] Janez Demšar. Statistical comparisons of classifiers over multiple data sets. *Journal of Machine learning research*, 7(Jan):1–30, 2006.
- [20] Madson L. D. Dias, César Lincoln C. Mattos, Ticiana L. C. da Silva, José Antônio F. de Macedo, and Wellington C. P. Silva. Anomaly Detection in Trajectory Data with Normalizing Flows. *arXiv:2004.05958 [cs, stat]*, April 2020.
- [21] Laurent Dinh, Jascha Sohl-Dickstein, and Samy Bengio. Density estimation using Real NVP. *arXiv:1605.08803 [cs]*, 2017.
- [22] Jeff Donahue, Philipp Krähenbühl, and Trevor Darrell. Adversarial feature learning. *arXiv:1605.09782 [cs]*, 2017.
- [23] Dheeru Dua and Casey Graff. UCI machine learning repository, 2017.
- [24] Andrew F. Emmott, Shubhomoy Das, Thomas Dietterich, Alan Fern, and Weng-Keen Wong. Systematic construction of anomaly detection benchmarks from real data. In *Proceedings of the ACM SIGKDD workshop on outlier detection and description*, pages 16–21, 2013.
- [25] Tolga Ergen and Suleyman Serdar Kozat. Unsupervised anomaly detection with lstm neural networks. *IEEE Transactions on Neural Networks and Learning Systems*, 31(8):3127–3141, Aug 2020.
- [26] Gilberto Fernandes, Joel JPC Rodrigues, Luiz Fernando Carvalho, Jalal F Al-Muhtadi, and Mario Lemes Proença. A comprehensive survey on network anomaly detection. *Telecommunication Systems*, 70(3):447–489, 2019.
- [27] Manuel Fernández-Delgado, Eva Cernadas, Senén Barro, and Dinani Amorim. Do we need hundreds of classifiers to solve real world classification problems? *The journal of machine learning research*, 15(1):3133–3181, 2014.
- [28] Mathieu Germain, Karol Gregor, Iain Murray, and Hugo Larochelle. MADE: Masked Autoencoder for Distribution Estimation. *arXiv:1502.03509 [cs, stat]*, June 2015.
- [29] Markus Goldstein and Andreas Dengel. Histogram-based outlier score (hbos): A fast unsupervised anomaly detection algorithm. *KI-2012: Poster and Demo Track*, pages 59–63, 2012.
- [30] Markus Goldstein and Seiichi Uchida. A comparative evaluation of unsupervised anomaly detection algorithms for multivariate data. *PloS one*, 11(4), 2016.
- [31] Ian Goodfellow, Jean Pouget-Abadie, Mehdi Mirza, Bing Xu, David Warde-Farley, Sherjil Ozair, Aaron Courville, and Yoshua Bengio. Generative adversarial nets. In *Advances in neural information processing systems*, pages 2672–2680, 2014.
- [32] Parikshit Gopalan, Vatsal Sharan, and Udi Wieder. Pidforest: Anomaly detection via partial identification. *arXiv:1912.03582 [cs]*, 2019.
- [33] Will Grathwohl, Ricky T. Q. Chen, Jesse Bettencourt, Ilya Sutskever, and David Duvenaud. FFJORD: Free-form Continuous Dynamics for Scalable Reversible Generative Models. *arXiv:1810.01367 [cs, stat]*, October 2018.
- [34] Ishaan Gulrajani, Faruk Ahmed, Martin Arjovsky, Vincent Dumoulin, and Aaron C. Courville. Improved training of wasserstein gans. In *Advances in neural information processing systems*, pages 5767–5777, 2017.
- [35] Stefan Harmeling, Guido Dornhege, David Tax, Frank Meinecke, and Klaus-Robert Müller. From outliers to prototypes: ordering data. *Neurocomputing*, 69(13-15):1608–1618, 2006.
- [36] Kaiming He, Xiangyu Zhang, Shaoqing Ren, and Jian Sun. Deep residual learning for image recognition. In *Proceedings of the IEEE conference on computer vision and pattern recognition*, pages 770–778, 2016.
- [37] Jennifer A Hoeting, David Madigan, Adrian E Raftery, and Chris T Volinsky. Bayesian model averaging: a tutorial. *Statistical science*, pages 382–401, 1999.
- [38] Yongjun Hong, Uiwon Hwang, Jaeyoon Yoo, and Sungro Yoon. How generative adversarial networks and their variants work: An overview. *ACM Computing Surveys (CSUR)*, 52(1):1–43, 2019.
- [39] Mike Innes. Flux: Elegant machine learning with julia. *Journal of Open Source Software*, 2018.
- [40] Tomoharu Iwata and Yuki Yamanaka. Supervised Anomaly Detection based on Deep Autoregressive Den-sity Estimators. *arXiv:1904.06034 [cs, stat]*, April 2019.

- [41] Diederik P. Kingma and Jimmy Ba. Adam: A method for stochastic optimization. *arXiv:1412.6980 [cs]*, 2017.
- [42] Diederik P. Kingma and Prafulla Dhariwal. Glow: Generative Flow with Invertible 1x1 Convolutions. *arXiv:1807.03039 [cs, stat]*, July 2018.
- [43] Diederik P Kingma and Max Welling. Auto-encoding variational bayes. *arXiv:1312.6114 [stat]*, 2014.
- [44] B Ravi Kiran, Dilip Mathew Thomas, and Ranjith Parakkal. An overview of deep learning based methods for unsupervised and semi-supervised anomaly detection in videos. *Journal of Imaging*, 4(2):36, 2018.
- [45] Polina Kirichenko, Pavel Izmailov, and Andrew Gordon Wilson. Why normalizing flows fail to detect out-of-distribution data. *arXiv:2006.08545 [stat]*, 2020.
- [46] Mark Kliger and Shachar Fleishman. Novelty detection with gan. *arXiv:1802.10560 [cs]*, 2018.
- [47] Ivan Kobyzev, Simon J. D. Prince, and Marcus A. Brubaker. Normalizing Flows: An Introduction and Review of Current Methods. *IEEE Transactions on Pattern Analysis and Machine Intelligence*, pages 1–1, 2020.
- [48] Hans-Peter Kriegel, Matthias Schubert, and Arthur Zimek. Angle-based outlier detection in high-dimensional data. In *Proceedings of the 14th ACM SIGKDD international conference on Knowledge discovery and data mining*, pages 444–452, 2008.
- [49] Alex Krizhevsky and Geoffrey Hinton. Learning multiple layers of features from tiny images. *University of Toronto*, 05 2012.
- [50] Donghwoon Kwon, Hyunjoo Kim, Jinoh Kim, Sang C Suh, Ikkyun Kim, and Kuinam J Kim. A survey of deep learning-based network anomaly detection. *Cluster Computing*, pages 1–13, 2019.
- [51] Yann LeCun and Corinna Cortes. MNIST handwritten digit database. 2010.
- [52] Fei Tony Liu, Kai Ming Ting, and Zhi-Hua Zhou. Isolation forest. In *2008 Eighth IEEE International Conference on Data Mining*, pages 413–422. IEEE, 2008.
- [53] Yezheng Liu, Zhe Li, Chong Zhou, Yuanchun Jiang, Jianshan Sun, Meng Wang, and Xiangnan He. Generative adversarial active learning for unsupervised outlier detection. *IEEE Transactions on Knowledge and Data Engineering*, 2019.
- [54] Alireza Makhzani, Jonathon Shlens, Navdeep Jaitly, Ian Goodfellow, and Brendan Frey. Adversarial autoencoders. *arXiv:1511.05644 [cs]*, 2016.
- [55] Annette M Molinaro, Richard Simon, and Ruth M Pfeiffer. Prediction error estimation: a comparison of resampling methods. *Bioinformatics*, 21(15):3301–3307, 2005.
- [56] Nour Moustafa, Jiankun Hu, and Jill Slay. A holistic review of network anomaly detection systems: A comprehensive survey. *Journal of Network and Computer Applications*, 128:33–55, 2019.
- [57] Eric Nalisnick, Akihiro Matsukawa, Yee Whye Teh, Dilan Gorur, and Balaji Lakshminarayanan. Do Deep Generative Models Know What They Don’t Know? *arXiv:1810.09136 [cs, stat]*, February 2019.
- [58] Yuval Netzer, Tao Wang, Adam Coates, Alessandro Bisacco, Bo Wu, and Andrew Y. Ng. Reading digits in natural images with unsupervised feature learning. In *NIPS Workshop on Deep Learning and Unsupervised Feature Learning 2011*, 2011.
- [59] Guansong Pang, Chunhua Shen, Longbing Cao, and Anton van den Hengel. Deep learning for anomaly detection: A review. *arXiv:2007.02500 [cs]*, 2020.
- [60] George Papamakarios, Eric Nalisnick, Danilo Jimenez Rezende, Shakir Mohamed, and Balaji Lakshminarayanan. Normalizing Flows for Probabilistic Modeling and Inference. *arXiv:1912.02762 [cs, stat]*, December 2019.
- [61] George Papamakarios, Theo Pavlakou, and Iain Murray. Masked Autoregressive Flow for Density Estimation. *arXiv:1705.07057 [cs, stat]*, June 2018.
- [62] F. Pedregosa, G. Varoquaux, A. Gramfort, V. Michel, B. Thirion, O. Grisel, M. Blondel, P. Prettenhofer, R. Weiss, V. Dubourg, J. Vanderplas, A. Passos, D. Cournapeau, M. Brucher, M. Perrot, and E. Duchesnay. Scikit-learn: Machine learning in Python. *Journal of Machine Learning Research*, 12:2825–2830, 2011.
- [63] Joao Pereira and Margarida Silveira. Unsupervised anomaly detection in energy time series data using variational recurrent autoencoders with attention. In *2018 17th IEEE International Conference on Machine Learning and Applications (ICMLA)*, pages 1275–1282. IEEE, 2018.
- [64] Pramuditha Perera, Ramesh Nallapati, and Bing Xiang. Ocgan: One-class novelty detection using gans with constrained latent representations. In *Proceedings of the IEEE Conference on Computer Vision and Pattern Recognition*, pages 2898–2906, 2019.
- [65] Tomáš Pevný. Loda: Lightweight on-line detector of anomalies. *Machine Learning*, 102(2):275–304, 2016.
- [66] Tomas Pevny, Vasek Smidl, Martin Trapp, Ondrej Polacek, and Tomas Oberhuber. Sum-product-transform networks: Exploiting symmetries using invertible transformations. *arXiv:2005.01297 [stat]*, 2020.
- [67] Stanislav Pidhorskyi, Ranya Almohsen, and Gianfranco Doretto. Generative probabilistic novelty detection with adversarial autoencoders. In *Advances in neural information processing systems*, pages 6822–6833, 2018.
- [68] Marco AF Pimentel, David A Clifton, Lei Clifton, and Lionel Tarassenko. A review of novelty detection. *Signal Processing*, 99:215–249, 2014.
- [69] Emanuele Principi, Fabio Vesperini, Stefano Squartini, and Francesco Piazza. Acoustic novelty detection with adversarial autoencoders. In *2017 International Joint Conference on Neural Networks (IJCNN)*, pages 3324–3330. IEEE, 2017.
- [70] Sridhar Ramaswamy, Rajeev Rastogi, and Kyuseok Shim. Efficient algorithms for mining outliers from large data sets. In *Proceedings of the 2000 ACM SIGMOD international conference on Management of data*, pages 427–438, 2000.
- [71] Jie Ren, Peter J. Liu, Emily Fertig, Jasper Snoek, Ryan Poplin, Mark A. DePristo, Joshua V. Dillon, and Bal-

- aji Lakshminarayanan. Likelihood Ratios for Out-of-Distribution Detection. *arXiv:1906.02845 [cs, stat]*, December 2019.
- [72] Olaf Ronneberger, Philipp Fischer, and Thomas Brox. U-net: Convolutional networks for biomedical image segmentation. In *International Conference on Medical image computing and computer-assisted intervention*, pages 234–241. Springer, 2015.
- [73] Lukas Ruff, Jacob R Kauffmann, Robert A Vandermeulen, Grégoire Montavon, Wojciech Samek, Marius Kloft, Thomas G Dietterich, and Klaus-Robert Müller. A unifying review of deep and shallow anomaly detection. *arXiv:2009.11732 [cs]*, 2020.
- [74] Lukas Ruff, Robert Vandermeulen, Nico Goernitz, Lucas Deecke, Shoaib Ahmed Siddiqui, Alexander Binder, Emmanuel Müller, and Marius Kloft. Deep one-class classification. In *International conference on machine learning*, pages 4393–4402, 2018.
- [75] Tim Salimans, Ian Goodfellow, Wojciech Zaremba, Vicki Cheung, Alec Radford, and Xi Chen. Improved techniques for training gans. In *Advances in neural information processing systems*, pages 2234–2242, 2016.
- [76] Thomas Schlegl, Philipp Seeböck, Sebastian M. Waldstein, Georg Langs, and Ursula Schmidt-Erfurth. F-AnoGAN: Fast unsupervised anomaly detection with generative adversarial networks. *Medical Image Analysis*, 54:30–44, May 2019.
- [77] Thomas Schlegl, Philipp Seeböck, Sebastian M Waldstein, Ursula Schmidt-Erfurth, and Georg Langs. Unsupervised anomaly detection with generative adversarial networks to guide marker discovery. In *International Conference on Information Processing in Medical Imaging*, pages 146–157. Springer, 2017.
- [78] Maximilian Schmidt and Marko Simic. Normalizing flows for novelty detection in industrial time series data. *arXiv:1906.06904 [cs, stat]*, June 2019.
- [79] Bernhard Schölkopf, John C Platt, John Shawe-Taylor, Alex J Smola, and Robert C Williamson. Estimating the support of a high-dimensional distribution. *Neural computation*, 13(7):1443–1471, 2001.
- [80] Vít Škvára, Tomáš Pevný, and Václav Šmídl. Are generative deep models for novelty detection truly better? *arXiv:1807.05027 [cs]*, 2018.
- [81] Vít Škvára, Václav Šmídl, Tomáš Pevný, Jakub Seidl, Aleš Havránek, and David Tskhakaya. Detection of alfvén eigenmodes on compass with generative neural networks. *Fusion Science and Technology*, pages 1–10, 2020.
- [82] Václav Šmídl, Jan Bím, and Tomáš Pevný. Anomaly scores for generative models. *arXiv:1905.11890 [stat]*, 2019.
- [83] Václav Šmídl, Jan Bím, and Tomáš Pevný. Orthogonal approximation of marginal likelihood of generative models. In *NIPS Workshop on Bayesian Deep Learning 2019*, 2019.
- [84] Ingo Steinwart, Don Hush, and Clint Scovel. A classification framework for anomaly detection. *Journal of Machine Learning Research*, 6(8):211–232, 2005.
- [85] Ilya Tolstikhin, Olivier Bousquet, Sylvain Gelly, and Bernhard Schoelkopf. Wasserstein auto-encoders. *arXiv:1711.01558 [stat]*, 2019.
- [86] Jakub Tomczak and Max Welling. VAE with a Vamp-Prior. In *International Conference on Artificial Intelligence and Statistics*, pages 1214–1223, 2018.
- [87] Régis Vert and Jean-Philippe Vert. Consistency and convergence rates of one-class svms and related algorithms. *Journal of Machine Learning Research*, 7(May):817–854, 2006.
- [88] Hongzhi Wang, Mohamed Jaward Bah, and Mohamed Hammad. Progress in outlier detection techniques: A survey. *IEEE Access*, 7:107964–108000, 2019.
- [89] Xuhong Wang, Ying Du, Shijie Lin, Ping Cui, Yuntian Shen, and Yupu Yang. advae: A self-adversarial variational autoencoder with gaussian anomaly prior knowledge for anomaly detection. *Knowledge-Based Systems*, 190:105187, 2020.
- [90] Andrew Gordon Wilson. The case for bayesian deep learning. *arXiv:2001.10995 [cs]*, 2020.
- [91] Han Xiao, Kashif Rasul, and Roland Vollgraf. Fashion-mnist: a novel image dataset for benchmarking machine learning algorithms. *arXiv:1708.07747 [cs]*, 2017.
- [92] Haowen Xu, Wenxiao Chen, Nengwen Zhao, Zeyan Li, Jiahao Bu, Zhihan Li, Ying Liu, Youjian Zhao, Dan Pei, Yang Feng, et al. Unsupervised anomaly detection via variational auto-encoder for seasonal kpis in web applications. In *Proceedings of the 2018 World Wide Web Conference*, pages 187–196, 2018.
- [93] Masataka Yamaguchi, Yuma Koizumi, and Noboru Harada. Adaflow: Domain-adaptive density estimator with application to anomaly detection and unpaired cross-domain translation. In *ICASSP 2019-2019 IEEE International Conference on Acoustics, Speech and Signal Processing (ICASSP)*, pages 3647–3651. IEEE, 2019.
- [94] Rong Yao, Chongdang Liu, Linxuan Zhang, and Peng Peng. Unsupervised Anomaly Detection Using Variational Auto-Encoder based Feature Extraction. In *2019 IEEE International Conference on Prognostics and Health Management (ICPHM)*, pages 1–7, San Francisco, CA, USA, June 2019. IEEE.
- [95] Houssam Zenati, Chuan Sheng Foo, Bruno Lecouat, Gaurav Manek, and Vijay Ramaseshan Chandrasekhar. Efficient gan-based anomaly detection. *arXiv:1802.06222 [cs]*, 2019.
- [96] Shengjia Zhao, Jiaming Song, and Stefano Ermon. Infovae: Information maximizing variational autoencoders. *arXiv:1706.02262 [cs]*, 2018.
- [97] Yue Zhao, Zain Nasrullah, and Zheng Li. Pyod: A python toolbox for scalable outlier detection. *Journal of Machine Learning Research*, 20(96):1–7, 2019.
- [98] Jun-Yan Zhu, Taesung Park, Phillip Isola, and Alexei A Efros. Unpaired image-to-image translation using cycle-consistent adversarial networks. In *Proceedings of the IEEE international conference on computer vision*, pages 2223–2232, 2017.
- [99] Bo Zong, Qi Song, Martin Renqiang Min, Wei Cheng, Cristian Lumezanu, Daeki Cho, and Haifeng Chen. Deep

autoencoding gaussian mixture model for unsupervised anomaly detection. In *International Conference on Learning Representations*, 2018.

APPENDIX A HYPERPARAMETER SETTINGS

An overview of sampled hyperparameters for all models used in our experiments is in Tab. A.1–A.3.

model	parameter	value set
ABOD	n method	$\{1, 2, \dots, 100\}$ fast
HBOS	no. bins α tolerance	$\{2, 4, \dots, 100\}$ $\{0.05, 0.1, \dots, 1\}$ $\{0, 0.05, \dots, 1\}$
IF	no. estimators max samples max features	$\{50, 100, \dots, 500\}$ $\{0.5, 0.6, \dots, 1\}$ $\{0.5, 0.6, \dots, 1\}$
kNN	n	$\{1, 3, \dots, 101\}$
LODA	no. bins no. cuts	$\{2, 4, \dots, 100\}$ $\{40, 60, \dots, 500\}$
LOF	n	$\{1, 2, \dots, 100\}$
OC-SVM	γ ν kernel	$10^x, x \in \{-4, -3.9, \dots, 2\}$ $\{0.01, 0.5, 0.99\}$ {rbf, sigmoid, polynomial}
PIDForest	max depth no. trees max samples max buckets ϵ	$\{6, 8, \dots, 10\}$ $\{50, 75, \dots, 200\}$ $\{50, 100, 250, 500, 1000, 5000\}$ $\{3, 4, 5, 6\}$ $\{0.05, 0.1, 0.2\}$

TABLE A.1: Hyperparameters of the classical models.

model	parameter	value set
MAF + RealNVP	h	$\{16, 32, \dots, 1024\}$
	no. flows	$\{2, 4, 8\}$
	η	10^{-4}
	batch size	$\{32, 64, 128\}$
	no. layers	$\{2, 3\}$
	activation	{relu, tanh}
	batch norm.	{true, false}
	init. identity.	{true, false}
	L_2 reg.	$\{0.0, 10^{-5}, 10^{-6}\}$
MAF	ordering	{natural, random}
RealNVP	tanh scaling	{true, false}
SPTN	no. components	$\{2, 4, 8, 16\}$
	batch size	$\{32, 64, 128\}$
	no. flows	$\{1, 2, 3\}$
	sharing	{dense, all, none}
	first dense	{true, false}
	activation	identity

TABLE A.2: Hyperparameters for the flow-based models.

APPENDIX B EXTENDING TABULAR EXPERIMENTS

Throughout the main text, we have reported only detailed results for the AUC metric, however for the sake of completeness we provide the underlying results of tabular experiments in TPR at 5% FPR using the *mean* protocol in Tab. B.1.

In Sec. IV-C we showed how the performance of different model types changes given the growing number of labeled samples in the validation set, however we have also investigated the same effect for the best performing representatives of

model	parameter	value set
common	$\dim(z)$	$\{8, 16, \dots, 256\}$
	h	$\{16, 32, \dots, 512\}$
	η	$\{10^{-4}, 10^{-3}\}$
	batch size	$\{32, 64, 128\}$
	activation	$\{\text{relu}, \text{swish}, \text{tanh}\}$
	no. dense layers	$\{3, 4\}$
	no. conv layers	$\{2, 3, 4\}$
	channels	$\{16, 32, 64, 128\}$
	kernelsizes	$\{3, 5, 7, 9\}$
WAE	scalings	$\{1, 2, 2, 2\}$
	λ	$\{0.1, 1\}$
	prior	$\{\mathcal{N}(\mathbf{0}, \mathbf{I}), \text{VampPrior}\}$
	K	$\{2, 4, \dots, 64\}$
	kernel	$\{\text{rbf}, \text{imq}, \text{rq}\}$
AAE	σ_k	$\{10^{-3}, 10^{-2}, 10^{-1}, 10^0\}$
	λ	$\{0.1, 1\}$
	prior	$\{\mathcal{N}(\mathbf{0}, \mathbf{I}), \text{VampPrior}\}$
	K	$\{2, 4, \dots, 64\}$
	no. discriminator layers	$\{1, 2, 3\}$
adVAE	α	$\{0, 0.1, \dots, 1\}$
	$\dim(z)$	$\{2, 4, \dots, 256\}$
	batch size	$\{32, 64\}$
	γ	$\{5 \cdot 10^{-4}, 10^{-3}, 5 \cdot 10^{-3}\}$
	λ	$\{5 \cdot 10^{-3}, 10^{-2}, 5 \cdot 10^{-2}\}$
	m_x	$\{1, 1.5\}$
	m_z	$\{40, 50, 60\}$
	decay	$\{0, 0.1, \dots, 0.5\}$
(skip)GANomaly	decay	$\{0, 0.1, \dots, 0.5\}$
	$w_{adv}, w_{con}, w_{enc}$	$\{1, 10, 20, \dots, 100\}$
	λ	$\{0.1, 0.2, \dots, 0.9\}$
	$R(x), L(X)$	$\{\text{MAE}, \text{MSE}\}$
	no. conv layers	$\{1, 2, 3, 4\}$
(fm)GAN	no. channels	$\{8, 16, \dots, 128\}$
	$\dim(z)$	$\{2, 4, \dots, 256\}$
	no. dense layers	$\{2, 3, 4\}$
DeepSVDD	α	$\{10^{-3}, 10^{-2}, \dots, 10^3\}$
	η_{AE}	$\{10^{-4}, 10^{-3}\}$
	batch norm.	$\{\text{true}, \text{false}\}$
	batch size	$\{64, 128\}$
	objective	$\{\text{soft boundary}, \text{one class}\}$
	ν	$\{0.01, 0.1, 0.5, 0.99\}$
fAnoGAN	decay	10^{-6}
	η_E	$\{10^{-4}, 10^{-3}\}$
	weight clip	$\{0.001, 0.005, 0.01, 0.05, 0.1\}$
	n_{critic}	5
	no. generator iterations	10000

TABLE A.3: Hyperparameters for the neural network based models.

each class, which may reveal different behaviour. As shown in Fig. B.1a, the trends are similar with OC-SVM (osvm), MAF (maf) and WAE (wae) having almost the same rank in the left region with the fewest number of labeled samples and OC-SVM improving its ranks at the expense of other methods. To complete the picture we also provide the same figure with TPR@5 metric, see Fig. B.1b, showing even more prominently the dominance of a properly tuned OC-SVM.

In order to demonstrate the scale of operations in this comparison study, Tab. B.2 and B.3 show the average number of trained models and score evaluations respectively trained and computed for each experimental repetition (fold).

APPENDIX C EXTENDING IMAGE EXPERIMENTS

Early in the work on image datasets we have realized that running the same number of repetitions per anomaly class as on tabular data is difficult with a given time budget, as for each hyperparameter 50 models must be trained. However the initial experiments suggested that the performance metrics when averaged over 10 anomaly classes are consistent across the repetitions, see Tab. C.1 showing AUC performance of VAE and GANomaly.

By default we used the *max* protocol when aggregating the results of the image experiments, as we have acknowledged that models of different expressiveness (thus different hyperparameters) are needed for each anomaly class problem. In Tab. C.2 and C.3 we provide results when using the *mean* protocol, which looks for hyperparameters with the best average performance on validation data across anomaly classes. In both settings the average ranks changed significantly with kNN (knn) and it's two stage variant VAE-kNN (vae) being the best method in the *leave-one-out* and the *leave-one-in* variants respectively. This may be attributed to kNN having more consistent performance on different problems for the same hyperparameter, though the difference from second and third best are not as pronounced. As opposed to the *max* protocol, standard deviations σ_1 of the best models are overall higher due to the fact, that some hyperparameters may perform worse on specific anomaly class problem.

The problem of varying performance on different anomaly classes becomes apparent when looking at each sub-problem as a separate dataset, shown in Tab. C.5 and C.6 for the *leave-one-out* and *leave-one-in* variants. Even though models with the same hyperparameters are trained for each anomaly class problem, a deeper look into the results, see Tab. C.4, shows that in the top 10 performing models by validation AUC the intersection of hyperparameters among different problems is minimal in the *leave-one-out* setting. In case of the *leave-one-in*, the situation is slightly different with classical methods sharing more.

On a related note, in Fig. C.1 the critical difference diagram of models trained in the *leave-one-out* setting, where each sub-problem is considered as a separate dataset, yielding higher confidence in the model differences.

In Fig. C.2a, C.2b we present how the best representatives of each model class perform under different level of knowledge about validation labels. As opposed to Fig. 4, where the results of GANs were comparable with autoencoders, the fmGAN performs on par with the best two-stage approach when the number of labeled samples in the validation set reaches hundreds.

In Sec. IV-A we claimed that models are sometimes more focused on the background instead of the semantic content of an image. This effect may be more pronounced in the *leave-one-in* configuration, which has fewer modalities. As an entertaining example we have devised a simple anomaly detector *blpix* for detecting the airplane class of the CIFAR10 dataset. As the name suggest it sums up all blue pixels in an image, resulting in anomaly score $s_{\text{blpix}}(x) = -\sum_{i,j} 1_{x_{i,j}=\text{blue}}$. De-

TABLE B.1: Performance of models on the tabular datasets with hyperparameter selection using the *mean* protocol on validation data, reported in the TPR@5 metric on the test data, averaged over 5 folds. σ_1 is the standard deviation for the best model over the folds, while σ_{10} is the average standard deviation of the best 10 models. The final row contains the average model rank.

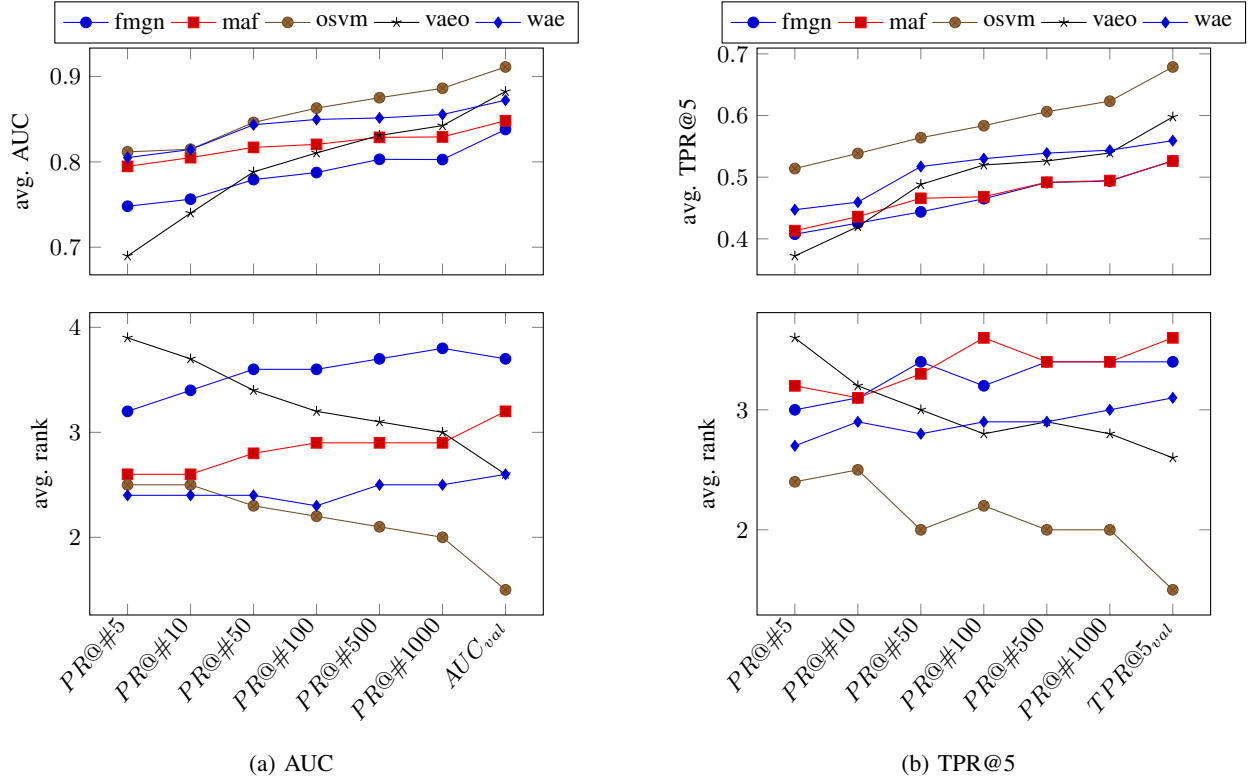


Fig. B.1: Average rank in AUC/TPR@5 against an increasing number of labeled samples measured by the PR@# n metric (precision at most n most anomalous samples on the validation data), as well as the ultimate knowledge of all labels encoded in AUC/TPR@5 on validation data, which are used as the criterion in the *mean* protocol. Only the best candidates of each model class are shown.

TABLE B.2: Average number of trained models per one experimental repetition (5 repetitions were done in total).

TABLE B.3: Average number of evaluated score functions per one experimental repetition.

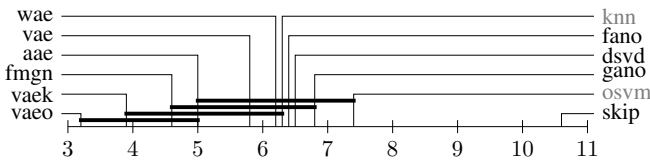


Fig. C.1: Critical difference diagram of models ranked via the AUC metric on the image data. $CD_{0.1}(12, 40) = 2.44$.

spite its simplicity, it achieves 0.68 AUC on both the validation and the test split, which is comparable with other models, see Fig. C.3.

More visual examples of anomalies for the best performing

models on image data are shown in Fig. C.4–C.7.

To illustrate the scale of operations in comparison of image models, the average number of trained models and score evaluation is presented in Tab. C.7 and C.8 respectively.

APPENDIX D ENSEMBLES EXPERIMENTS

Creation of ensembles consisted of two steps. Firstly the performance metrics were precomputed for all the methods and each repetition or anomaly class, in order to quickly assert which hyperparameters to include. Secondly we created multiple ensembles for each combination of the criterion metric and size, totaling in 4 different ensembles per each

(a) VAE

(b) GANomaly

TABLE C.1: Summary tables for the VAE and GANomaly models on different seeds of the image datasets. Reported values are the AUC metrics on the test data, averaged over 10 anomaly classes.

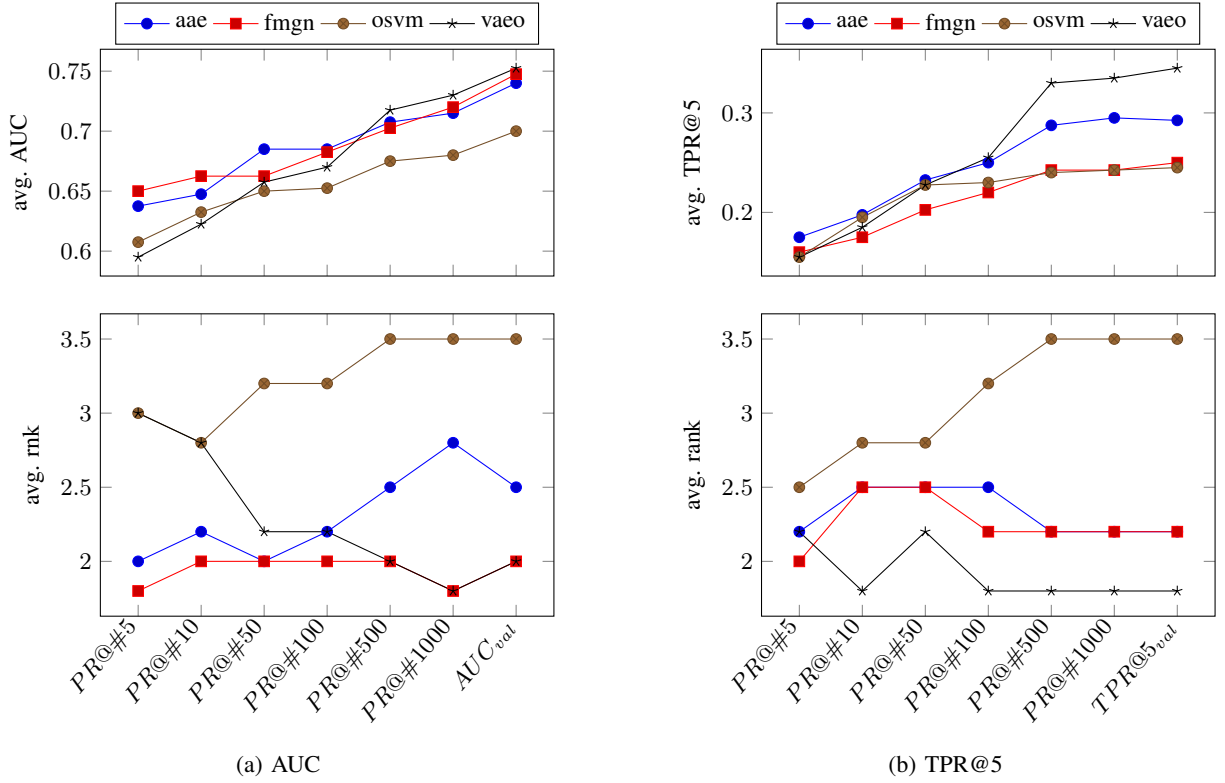


Fig. C.2: Average rank in the AUC/TPR@5 metrics against increasing the number of labeled samples measured by the PR@# n metric (precision at most n most anomalous samples on validation data), as well as the ultimate knowledge of all labels encoded in the AUC/TPR@5 on the validation data, which are used as the criterion in the *max* protocol. Only the best candidates of each model class are shown.

TABLE C.2: Summary table for the image data using the *leave-one-out* strategy and the *mean* protocol. Reported are the AUC values on the test data, averaged over 10 anomaly classes. σ_1 is the standard deviation for the best model over the folds, while σ_{10} is the average standard deviation of the best 10 models. Last row shows ranks derived using the *max* protocol used by default on the image datasets.

TABLE C.3: Summary table for the image data using the *leave-one-in* strategy and the *mean* protocol. Reported are the AUC values on the test data, averaged over 10 anomaly classes. σ_1 is the standard deviation for the best model over the folds, while σ_{10} is the average standard deviation of the best 10 models. Last row shows ranks derived using the *max* protocol used by default on the image datasets.

repetition/anomaly class. During evaluation the best ensembles were selected by the *max* protocol on the validation data, as the *mean* does not make much sense.^{D.1} Resulting average ranks in the AUC metric and average improvement in the AUC are presented in the last rows of Tab. D.1 and D.3 for the tabular and image data, respectively. The effect of the sorting criterion and the size of an ensemble is shown in the same place, suggesting that smaller ensembles on tabular data perform better, though we are inclined to state that the ensembles we tried degrade performance of some methods less than for other. Additionally Tab. D.1 and D.3 show the same results when measured in TPR@5. Needless to say the performance is lower when the criterion and evaluation metric are mismatched, though the value of AUC is in this regard better.

^{D.1}Hyperparameters such as the criterion do not define the contents of an ensemble, only the means of its creation, therefore ensembles with the same hyperparameters across repetitions do not necessarily contain the same models, which in turn does not fit with the *mean* protocol.

dataset	aae	knn	gano	vae	osvm	fmgn	skip	vaeo	wae	fano	vaeo	dsvd
cifar10	0	0	0	0	0	0	0	0	0	0	0	0
fmnist	0	0	0	0	0	0	0	0	0	0	0	0
mnist	0	0	0	0	0	0	0	0	0	1	0	0
svhn2	0	2	0	0	0	0	0	0	0	0	0	0

(a) *leave-one-out*

dataset	aae	knn	gano	vae	osvm	fmgn	skip	vaeo	wae	fano	vaeo	dsvd
cifar10	0	0	0	0	0	0	0	0	0	0	0	0
fmnist	0	0	0	0	4	2	0	0	0	0	0	0
mnist	0	6	0	0	7	0	0	0	0	2	0	3
svhn2	0	7	0	0	10	3	0	0	0	1	2	4

(b) *leave-one-in*

TABLE C.4: Size of the intersection of the top 10 performing hyperparameters in AUC on validation data.

TABLE C.5: Summary table of the AUC metric for the image data when anomaly class problem is treated as a separate dataset in the *leave-one the-out* setting.TABLE C.6: Summary table of the AUC metric for the image data when anomaly class problem is treated as a separate dataset in the *leave-one-in* setting.

TABLE C.7: Average number of trained models per one anomaly class (10 anomaly classes were used in total).

APPENDIX E

IMPLEMENTATION DETAILS

A. Classical methods

Due to the quadratic scaling of OC-SVM with the number of training samples, on image data, we have implemented the OC-SVM as an ensemble of 10 OC-SVM models with the same hyperparameters but trained on 10 same-size subsets of training data. The anomaly score was then the average of anomaly scores of the members of the ensemble.

For the kNN model, we have used 3 anomaly scores that differed at the distance computation, as described in [35].

The original PIDForest [32] method’s implementation provided scikit-learn model API, however that’s where the convenience ended. We have encountered a number of errors both during training and prediction, some of which we have identified were caused by features with constant values, which we had to filter out from the splits, before proceeding. It’s quite unfortunate when, what seems to be a sound method on paper, is handicapped by a subpar implementation, which is both slow and breaks at the first sight of the unknown. Though the authors have promised a better one, as of the time of writing, such an option was not available. As opposed to the original implementation we used negative sparsity as the anomaly score and parametrized its quantiles at three levels $\{0.05, 0.1, 0.2\}$.

B. Autoencoders & GANs

The training of VAE, WAE and AAE models has been stopped prematurely if the loss on the validation dataset has not improved for 200 batches. For GAN and fmGAN, patience of 50 batches was used and the discriminator loss was used for early stopping. We have not used batch normalization in any of these models, as it is recommended not to do so due to the additional stochasticity that it introduces in the training process.

In the construction of VAE, WAE, AAE, GAN and fmGAN models on image data, convolution layers are used. First the number of convolution layers n_c was sampled. To construct decoder/generator parts, the first n_c elements of the channels, kernelsizes and scalings vectors in Tab. A.3 were used, e.g. for $n_c = 2$, a decoder with (16,32) channels, (3,5) kernelsizes and (1,2) scaling was constructed, while the architecture of the encoder/discriminator was flipped. Downscaling in encoders/discriminators was done with maxpooling, upscaling in decoders/discriminators was done via transposed convolutions.

Each of the k components of a VampPrior initialized with an average sample of the training data, perturbed with noise sampled from $\mathcal{N}(0, 1)$ in each dimension.

The most challenging was the implementation of ad-VAE [89] because there was no training loop or loss functions in the code provided by the author. In addition, the other implementation recommended by the author differs from the paper in terms of loss functions and some hyperparameters. However, we managed to implement a working version of the model that follows the paper as closely as possible. The only difference is the architecture of the encoder and decoder.

In the case of GANomaly and skip-GANomaly for image data, we implemented the exact same architectures as in original papers [2, 3] and the only addition to those models is weight decay. This architecture, which is pretty much similar for both models, has one small disadvantage. The width of the input image must be equal to its height and that must be divisible by 32. This allows fully convolution encoders to compress input image into 1D latent vector resp. $(1, 1, \dim(z))$ tensor. Therefore we have to resize MNIST and FashionMNIST datasets in the preprocess phase from shape 28x28 to 32x32.

To avoid overfitting of deep models we decided to use an early stopping procedure. The criterion for this procedure most often corresponds to the anomaly score formula or loss function, so it is different for every model. For exam-

TABLE C.8: Average number of evaluated score functions per one anomaly class.

TABLE D.1: Comparison of the average AUC ranks and average change in the AUC with different ensemble sizes and criterion used for their selection for the tabular data. Rows with values in blue show average improvement in AUC from the baseline.

TABLE D.2: Comparison of the average TPR@5 ranks and average change in the TPR@5 with different ensemble sizes and criterion used for their selection for tabular data. Rows with values in blue show average improvement in AUC from the baseline.

TABLE D.3: Comparison of average AUC ranks and average change in the AUC with different ensemble sizes and criterion used for their selection for the image data. Average change shows average improvement in AUC from the baseline.

ple GANomaly’s early stopping criterion is simple generator loss $L_G = w_1 L_{adversarial} + w_2 L_{contextual} + w_3 L_{latent}$ [2], however for skip-GANomaly we use weighted average of generator loss L_G and discriminator loss L_D because both those terms are also part of anomaly score. Weights in L_G are typically treated as hyperparameters which we sample. Exception is image version of GANomaly where we used fixed weights $w_1 = 1$, $w_2 = 50$ and $w_3 = 1$ since those weights were empirically derived in original paper as optimal for the same datasets we use.

During the implementation of fAnoGAN (resp. f-AnoGAN) we were forced to make some adjustments to the original code. Firstly we switched Wasserstein GAN with gradient penalty (WGAN-GP [34]) to its predecessor WGAN with clipping weights [5] because we were not able to compute the second order derivative needed to update weights of the model due to Julia limitations. Later we tried Pytorch implementation of WGAN-GP, but it performed on par with WGAN so we dropped it from results.

Secondly, we exchanged original ResNet [36] generator and discriminator to a much lighter architecture (similar to GANomaly) we also use for autoencoders. This helps to compare models more fairly, as their performance now depends mainly on the model concept, not the architecture. In addition, fAnoGAN is the only model without an early stopping procedure, because its loss behavior is not standard and we had a hard time figuring out when to stop it.

C. Normalizing flows

While implementing RealNVP and MAF flows on tabular data we tried to follow as closely as possible the code that has accompanied [61], however on a closer inspection, we found that there is a lot of variety in the literature, which we tried to include into hyperparameters of each of the methods. This variety comes mainly from the different techniques, that authors [21, 33, 42] employ to battle instabilities in the training of deep flows, though the exact nature of which is often not disclosed. In our case, the root of most problems was in scale conditioner’s output saturating (yielding Inf) in the

subsequent exponentiation. We have been able to isolate this to specific samples in the training datasets such as Statlog Shuttle, which unfortunately contained outliers with one of the features having disproportional values. The MAF flows seemed to be more affected by this due to their autoregressive structure, which propagated the discrepancy into other features in each subsequent flow.

Using batch normalization as suggested by [61] should supposedly improve both stability and target likelihoods, which we could confirm while experimenting on small problems, however it did not help us with the aforementioned issues. We’ve found that batch normalization with floating averages as used in [21] performed poorly even on smaller problems, thus we used only statistics computed for each batch individually. While looking deeper into the performance of different hyperparameters, we have found that none of the models on KDD99 (10%) with batch normalization trained properly yielding AUC’s below 0.5. As per the original implementation, during evaluation the statistics in batch normalization were initialized from the whole training dataset.

As suggested by [21] we have also experimented with initializing the flow to identity by zeroing the last layers of conditioner networks, however it also did not help. Furthermore in case of RealNVP flow we have tried to use “tanh normalization” together with learn-able location $\alpha_s \in \mathbb{R}$ and scale $\beta_s \in \mathbb{R}$ parameters

$$\alpha_s \oplus \exp \beta_s \odot \tanh(s), \quad (16)$$

where s is the scale conditioner’s output and \oplus , \odot are element-wise operations. Using this scaling together with tanh activations, we were able to train even deeper and wider architectures.

One of the degrees of freedom is the choice of conditioner architecture. Where on images the consensus [21, 42] seems to be to use one convolution neural network for both location and scale parameters and feeding the network positive and negative input. In the case of tabular flows, where the number of weights is not as closely controlled variable, the additional options are to employ either two networks for both scale and

TABLE D.4: Comparison of average TPR@5 ranks and average change in the TPR@5 with different ensemble sizes and criterion used for their selection for tabular data. Average change shows average improvement in the TPR@5 from the baseline.

location (RealNVP implementation in[61]), or one network whose output is fed through another pair of single-layer networks to provide the two outputs (MAF implementation in[61]). We have opted for using two separate networks for both RealNVP/MAF flows to equal the situation.

Even the exact formulation transformation function f from (1) has different forms in the chosen class of autoregressive affine flows [60], across different implementations. We have used the following definition of forward step f^{-1} for RealNVP

$$\begin{aligned} z_{\leq d} &= \mathbf{x}_{\leq d}, \\ z_{> d} &= \exp\left(-\frac{1}{2}\mathbf{s}\right) \odot (\mathbf{t} - \mathbf{x}_{\leq d}), \end{aligned} \quad (17)$$

where \mathbf{s} , \mathbf{t} are outputs of scale and location conditioners respectively when given the first half of the input $\mathbf{x}_{\leq d} = \mathbf{z}_{\leq d}$. In case of MAF flow the forward step had the following form

$$z_i = \exp\left(-\frac{1}{2}s_i\right) (t_i - x_i), \quad \forall i \in \{1, \dots, D, \} \quad (18)$$

where s_i , t_i are the i -th elements of outputs of the autoregressive conditioners (MADE networks [28]) for scale and location parameters respectively, when given the whole input vector \mathbf{x} . It is important to stress the halving of the outputs of the scale conditioners, as this is another means with which to battle the aforementioned instabilities.

Lastly, we have used the same training loop for both flows with early stopping and patience at 200, checking at every iteration, same as in [61].

Adopting the code of SPTN flows was easier, as it has been already written in Julia and the only changes we have made were in the training loop. We have used early-stopping, though due to the high cost of evaluation of validation loss, we have opted for patience 20 and checking interval 10. Note also that on higher-dimensional datasets — HAR, Letter Recognition, Isolet, Multiple Features, Arrhythmia — the implementation did not allow us to compute all 5 repetitions and therefore only the minimum of 3 has been completed.

D. Evaluation

Though we have been meticulous in the implementation, due to the scale of operation we could not cover all the edge cases and therefore some runs did not complete at all or produced corrupted results with invalid values. When a method produced scores with more than half of the values being NaN, such results were filtered out. Overall less than 0.5% (11k) of results from the tabular experiments have been affected, out of which the majority (10k) have come from our kNN implementation on small dimensional datasets, where only low values of k produced a valid result. Results on the image datasets did not contain any invalid values.

As a result, the experimental files for some combinations of hyperparameter-seed-model were missing and had to be

handled in the later stages of evaluation. In this sense *mean* protocol is more strict as it required at least 3 repetitions of each hyperparameter for tabular data and all anomaly classes in the case of image datasets. On the other hand *max* checks only the edge cases where there are no results for repetition/anomaly class, therefore even one sample per repetition/anomaly class each with different hyperparameter is acceptable, though this has never happened.

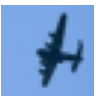


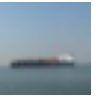

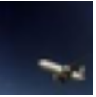


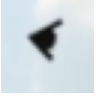

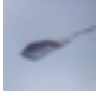

Model	Examples										AUC
blpix											0.68
vae											0.70
vaeo											0.75
vaek											0.71
aae											0.69
wae											0.68
gano											0.62
skip											0.33
osvm											0.72
knn											0.69
fmgn											0.80
fano											0.77
dsvd											0.76

Fig. C.3: CIFAR10 images with the lowest anomaly scores (*most normal*) for each model. Models were trained only on airplane images (*leave-one-in*). Blpix is a detector based on the number of blue pixels.

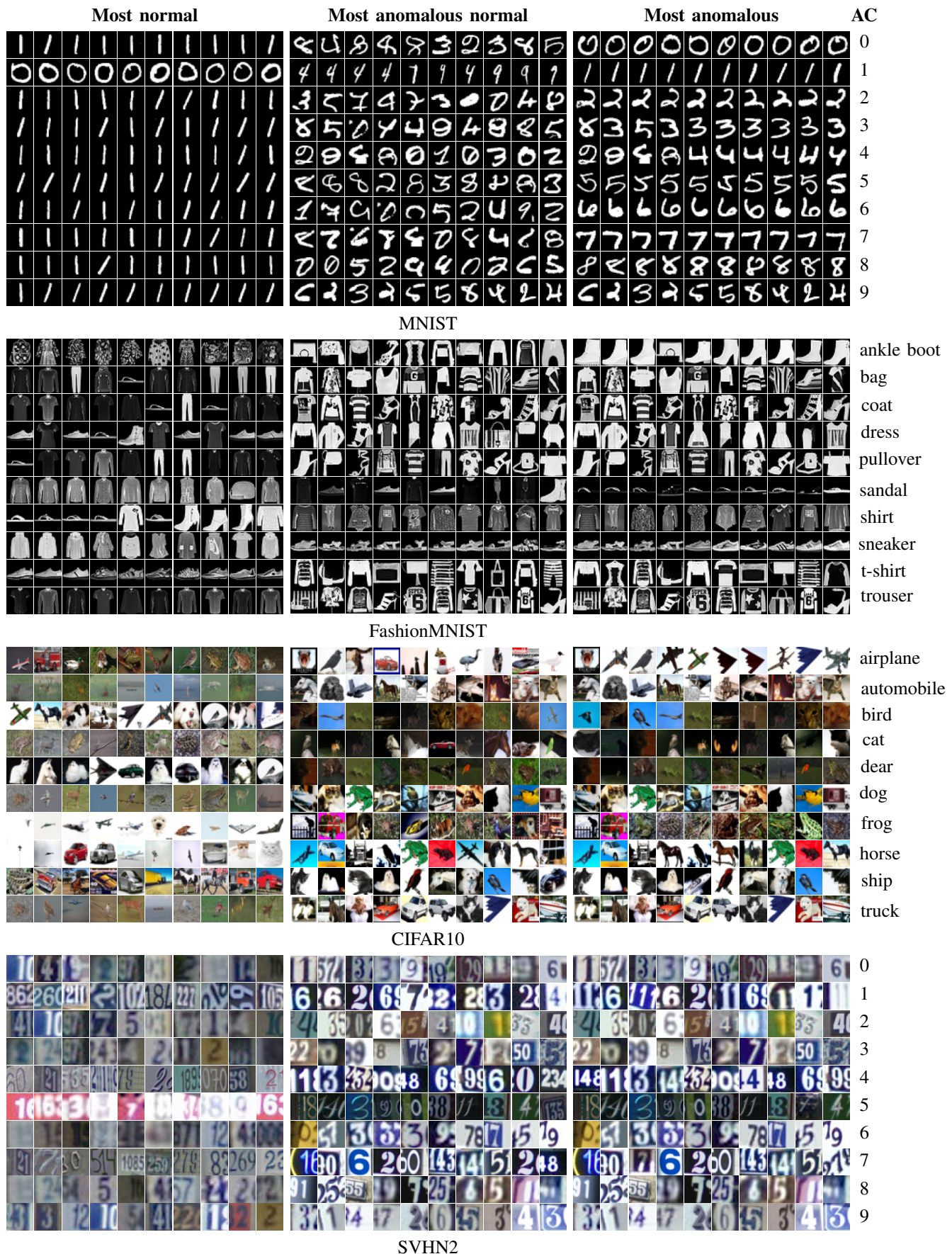


Fig. C.4: Examples of the best performing model VAE-OCSVM (vaeo) with *leave-one-out*. AC means anomaly class that was omitted from the training

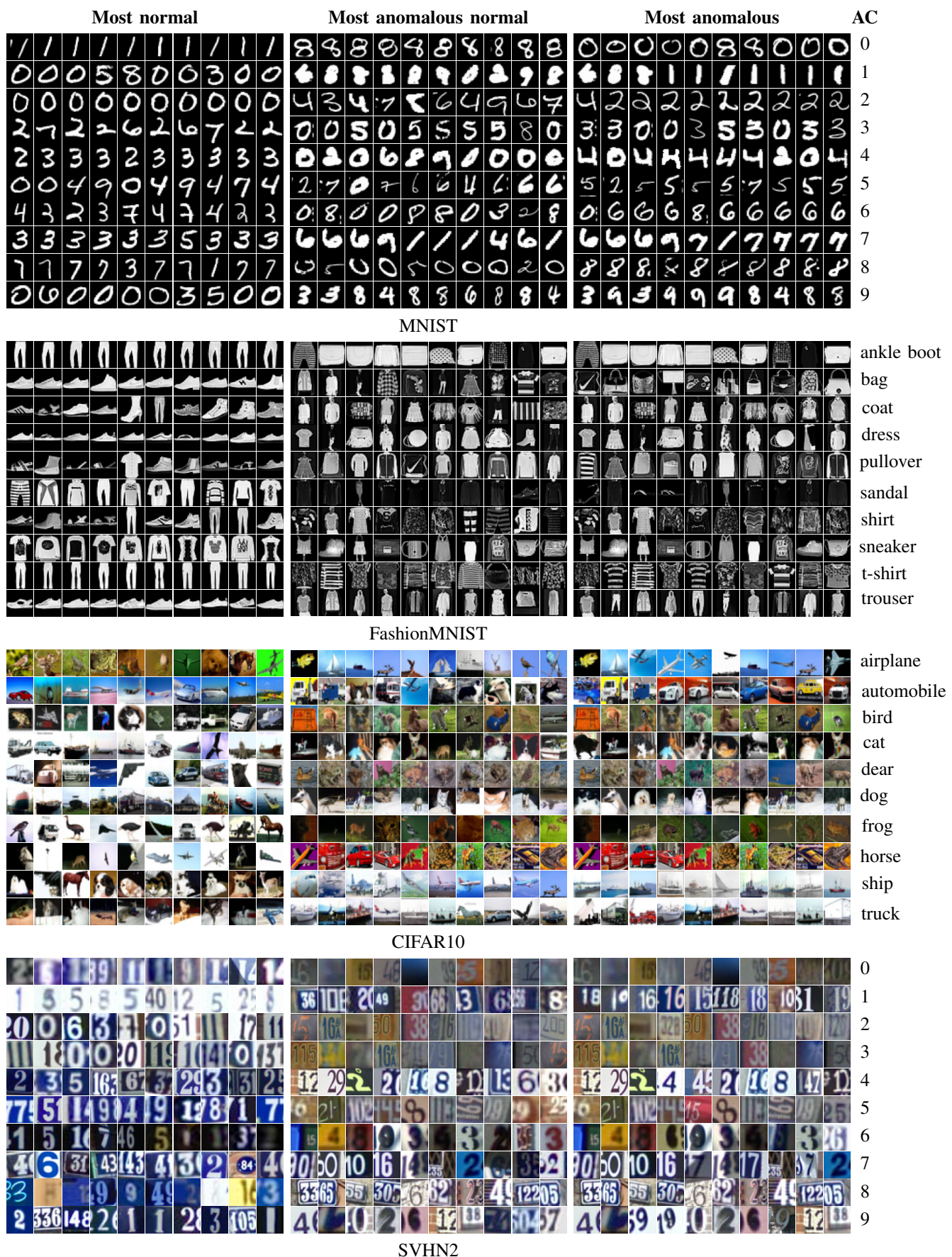


Fig. C.5: Examples of the second-best performing model fmGAN (fmgn) with *leave-one-out*. AC means anomaly class that was omitted from the training

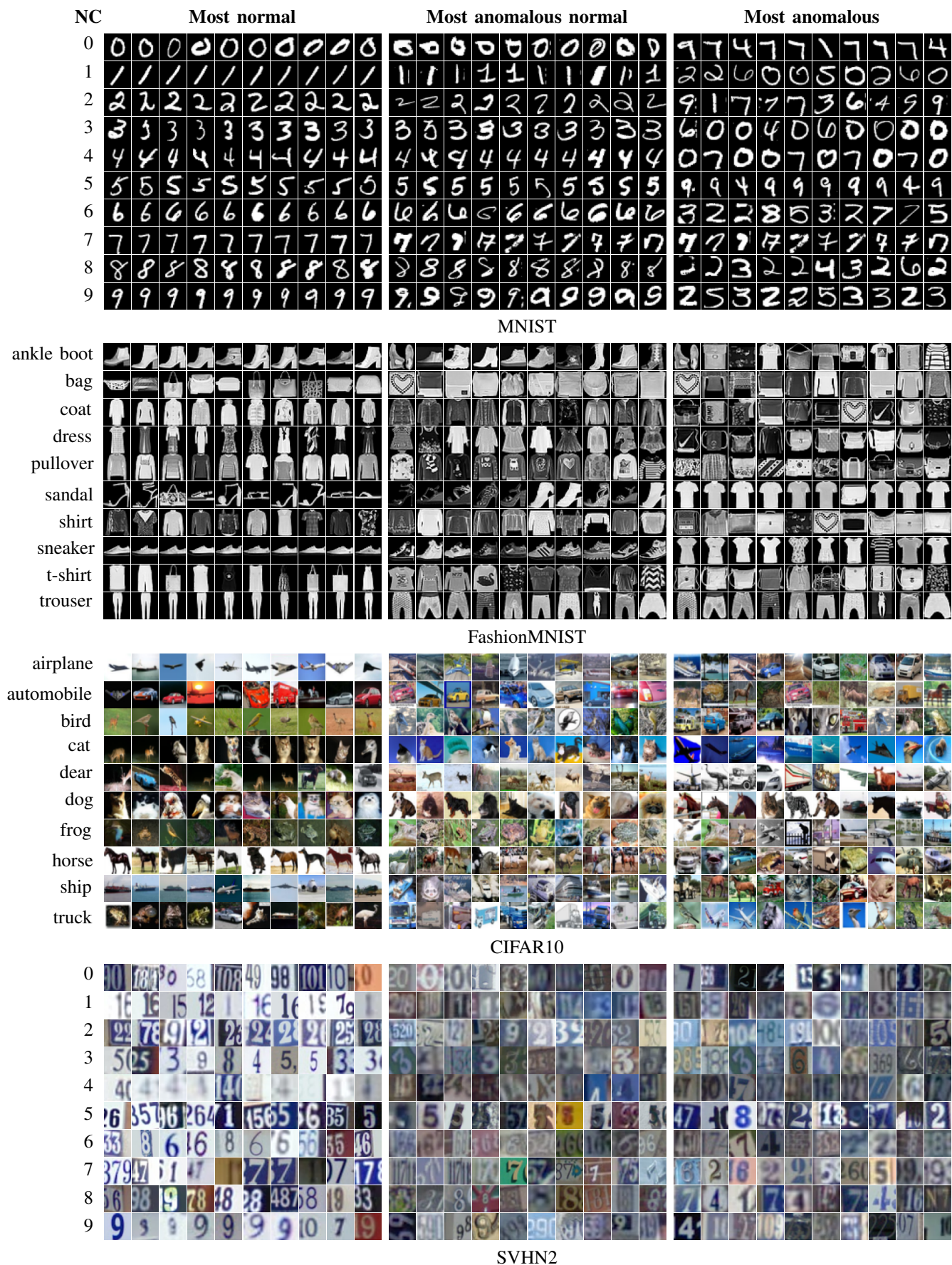


Fig. C.6: Examples of fmGAN (fmgn) with *leave-one-in*. NC means normal class on which the models were trained.

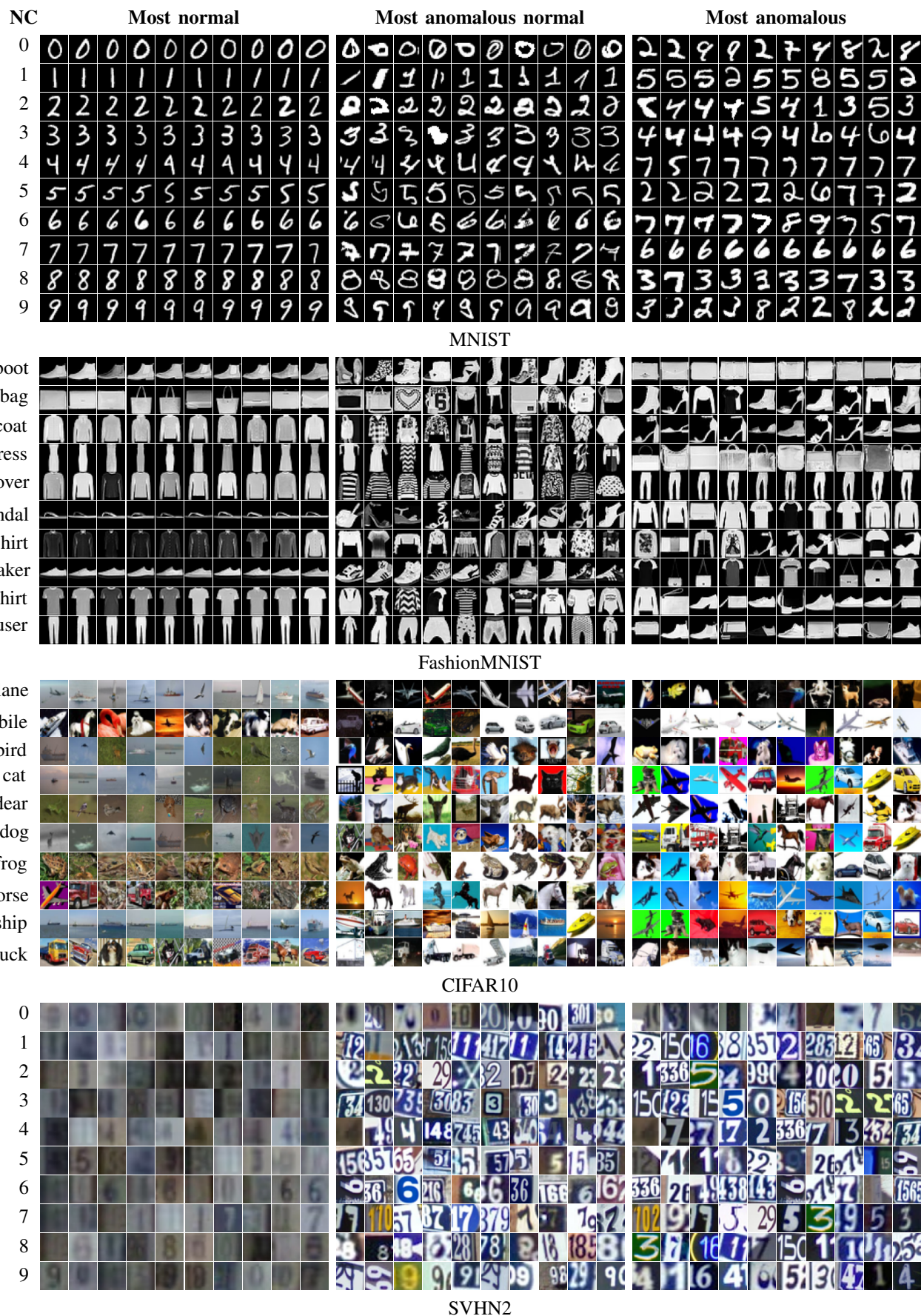


Fig. C.7: Examples of VAE with *leave-one-in*. NC means normal class on which the models were trained